June 18, 2014
TPF-5(264) Passive Force/Skewed Abutments
Task 9 Preliminary Report

TASK 9 REPORT

PASSIVE FORCE-DEFLECTION TESTS FOR REINFORCED CONCRETE WINGWALL SKEWED ABUTMENTS

Prepared By

Kyle M. Rollins, Professor, Civil & Env. Engrg Dept., Brigham Young Univ., 368 CB, Provo, UT 84602, (801) 422-6334, rollinsk@byu.edu

Ian Oxborrow, Research Asst., Civil & Env. Engrg Dept., Brigham Young Univ., 368 CB, Provo, UT 84602; i.oxborrow@gmail.com

Kyle Smith, Research Asst., Civil & Env. Engrg Dept., Brigham Young Univ., 368 CB, Provo, UT 84602, kyle.smith@byu.net

Amy Fredrickson, Research Asst., Civil & Env. Engrg Dept., Brigham Young Univ., 368 CB, Provo, UT 84602, af711.byu@gmail.com

Arthur Guo, Research Asst., Civil & Env. Engrg Dept., Brigham Young Univ., 368 CB, Provo, UT 84602, gzifan@gmail.com

Prepared for

Research Division of the Utah Department of Transportation

June 18, 2014

EXECUTIVE SUMMARY

Accounting for seismic forces and thermal expansion in bridge design requires an accurate passive force-deflection relationship for the abutment wall. Current design codes make no allowance for skew effects on passive force; however, quarter scale lab tests indicate that there is a significant reduction in peak passive force as skew angle increases for plane-strain cases. To further explore this issue larger scale field tests were conducted with skew angles of 0° and 45° with longitudinal, reinforced-concrete wingwalls. The abutment backwall was 11-ft (3.35-m) wide by 5.5-ft (1.68-m) high and backfill material consisted of dense compacted sand. The peak passive force for the 45° skew test was found to be 50% of the peak passive force for the 0° skew case. Longitudinal displacement of the backwall at the peak passive force was found to be between 4% and 5% of the backwall height for the 0° and 45° skew test which is consistent with previously reported values for large-scale passive force-deflection tests. Passive pressure across the backwall was typically lower near the center of the wall and higher at the edges with the highest pressures at the acute corner. Shear force on the backwall increased as skew angle increased despite the reduction in longitudinal force with skew angle. Transverse pile cap displacements also increased with skew angle and were sufficient to mobilize the frictional resistance. Heave geometries for the 0° and 45° tests were 2% to 4% of the fill height.

INTRODUCTION

Several large-scale field tests have investigated passive force-deflection behavior with densely compacted granular backfills (Cole and Rollins 2006; Duncan and Mokwa 2001; Lemnitzer et al. 2009; Rollins and Sparks 2002). Results of numerous field studies indicate that peak passive force is adequately predicted using the log-spiral method, typically achieved at displacements approximately 3% to 5% of the backwall height (Cole and Rollins 2006; Lemnitzer et al. 2009). Methods of approximating passive force-deflection curves with a hyperbola have been developed by Duncan and Mokwa (2001) and Shamsabadi et al. (2006, 2007). However, for simplicity in design, most bridge design specifications recommend a bilinear relationship (AASHTO 2011; Caltrans 2010).

Until recently, no large-scale experiments had been conducted to determine the passive force-deflection relationships for skewed bridge abutments. Furthermore, current bridge design practices assume the peak passive force is the same for skewed bridges as for non-skewed bridges (AASHTO 2011). However, field evidence clearly indicates poorer performance of skewed abutments during seismic events (Apirakyorapinit et al. 2012; Elnashai et al. 2010; Shamsabadi et al. 2006; Unjohn 2012) and distress to skewed abutments due to thermal expansion (Steinberg and Sargand 2010). Laboratory tests performed by Rollins and Jessee (2012) and numerical analyses performed by Shamsabadi et al. (2006) both found that there is a significant reduction in passive force as skew angle increases. Using data obtained from these studies, Rollins and Jessee (2012) proposed the correction factor, R_{skew}, given by Equation (1) which defines the ratio between the peak passive force for a skewed abutment ($P_{P\text{-}skew}$) and the peak passive force for a non-skewed abutment ($P_{P\text{-}no\ skew}$) as a function of skew angle, θ.

$$\mathrm{R_{skew}} = \frac{P_{p-skew}}{P_{p-no\ skew}} = 8.0 * 10^{-5}\theta^2 - 0.018\theta + 1.0 \qquad (1)$$

Because Equation (1) is based only on small-scale tests and computer models with plane-strain conditions, the need for additional large-scale testing with more realistic boundary conditions was apparent. For this study, two large-scale field tests were performed with skew angles of 0° and 45° using an existing pile cap and reinforced concrete wingwalls connected to the pile cap with concrete wedge

anchors. The pile cap was 15-ft (4.6-m) long, 11-ft (3.4-m) wide and 5.5-ft (1.7-m) high and has been used in several past field studies (Rollins and Sparks 2002; Rollins et al. 2010; Strassburg 2010). Concrete wedges were attached to the face of the pile cap to create the skewed geometry necessary for testing.

Although passive force-deflection behavior for non-skewed abutments with reinforced concrete wingwalls has been investigated previously (Bozorgzadeh et al. 2008; Romstad et al. 1996), to the author's knowledge, the structural and geotechnical response of the wingwalls have not been published. This paper presents test configuration and procedures, results for abutment, backfill and wingwalls, and conclusions based on analysis of the test results.

BACKGROUND

As outlined by Burke Jr. (1994) and shown in Figure 1, the interaction of forces at the interface between the bridge abutment backwall and soil backfill may be expressed in terms of the total longitudinal force, P_L, and its components normal to and transverse to the abutment. The normal force is resisted by the passive force, P_P [see Equation (2)]; and the transverse, or shear force, P_T [see Equation (3)], is resisted by the shear resistance, P_R [see Equation (4)]. To prevent instability of the bridge caused by sliding of the abutment against the soil backfill the inequality shown in Equation (5) must be satisfied. In addition, rotation of the entire bridge can occur if the inequality in Equation (6) is not satisfied.

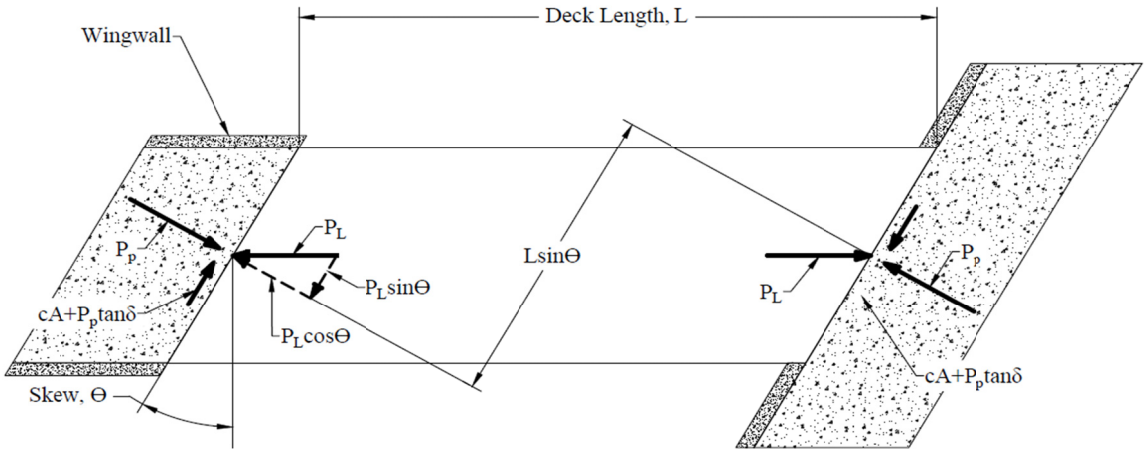

Figure 1. Typical distribution of forces on a bridge with skewed abutments.

$$P_P = P_L \cos\theta \tag{2}$$

$$P_T = P_L \sin\theta \tag{3}$$

$$P_R = cA + P_P \tan\delta \tag{4}$$

$$\frac{cA + P_P \tan\delta}{F_s} \geq P_L \sin\theta \tag{5}$$

$$\frac{(cA + P_P \tan\delta) L \cos\theta}{F_s} \geq P_P L \sin\theta \tag{6}$$

where

$\theta =$ skew angle of backwall

$c =$ soil cohesion

$A =$ backwall area

$\delta =$ angle of friction between backfill soil and abutment wall

$F_s =$ factor of safety

$L =$ length of bridge

These equations are only strictly valid if the bridge remains stable; therefore, if the bridge rotates, the distribution of forces on the abutment backwall will likely change, rendering these equations less accurate. Based on Equation (6), Burke Jr. (1994) noted that if cohesion is ignored the potential for bridge rotation is independent of passive force and bridge length so that at a typical design interface friction angle of 22°, the factor of safety decreases to below 1.5 if bridge skew exceeds 15°.

Test configuration for this study closely resembled the left end of the bridge in Figure 1 with longitudinal reinforced concrete wingwalls. Two previous studies investigated force-deflection behavior of abutments with reinforced concrete wingwalls. Romstad et al. (1996) performed cyclic load-displacement tests on a non-skewed abutment with integral wingwalls with Yolo Loam (clayey silt) and well-graded silty sand as the embankment and structural backfill material, respectively. They reported passive force-deflection and stiffness-displacement results with the peak passive force (P_{peak}) mobilizing

at displacements approximately 8% of the backwall height. A similar study was done by Bozorgzadeh et al. (2008), with silty sand as both the embankment and backfill material, where P_{peak} was achieved at approximately 2% to 3% of the backwall height; however, in this case the wall was not constrained against upward movement by piles . To the author's knowledge, no results were reported in either study regarding wingwall response.

TEST CONFIGURATION

Test Geometry

The test setup for the previous small-scale laboratory tests involved a 2 ft (0.61 m) high by 4 ft (1.22 m) wide backwall with a 2D or plane-strain backfill geometry, as shown in Figure 2 (Rollins and Jessee 2012). In contrast, the field tests used an existing 11 ft (3.35 m) wide by 5.5 ft (1.68 m) high by 15 ft (4.57 m) long pile cap to simulate an abutment backwall as shown in Figure 3. Reinforced concrete wingwalls extend 6 ft into the backfill on both sides of the pile cap. Instead of a 2D backfill geometry, the backfill was placed in a test pit that extended a little over 5 ft (1.52 m) out from the sides of the pile cap to the edge of the test pit to allow for the development of a 3D failure geometry. The backfill extended 24 ft (7.32 m) longitudinally from the face of the backwall and approximately 1 ft (0.30 m) below the bottom of the backwall within 10 ft of backwall face to contain the potential failure surface. Outside the total abutment width (including wingwalls) and beyond 24 ft outward from the backwall, the backfill tapered downward at a 2H:1V slope to simulate typical field conditions Though the native soil was significantly stiffer than the backfill materials, the backfill boundaries were considered to be far enough away to not affect the development of a shear surface. Beyond 10 ft (3.05 m), the base of the backfill tapered up to be approximately even with the base of the cap to reduce the required backfill volume.

Load was applied in the longitudinal direction with two 600-kip (2,670 kN) hydraulic actuators which reacted against a sheet pile wall and two 4-ft (1.22 m) diameter drilled shafts that were coupled together by two deep beams.

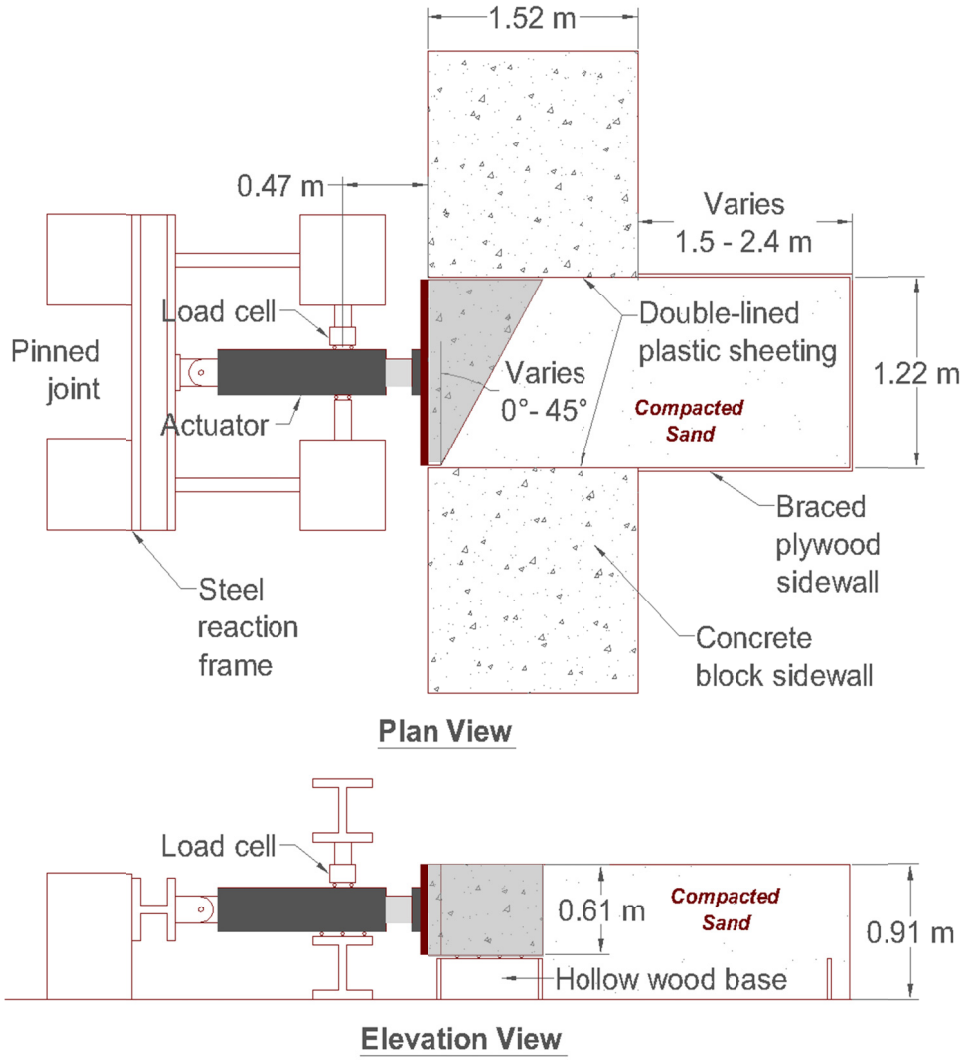

Figure 2. Schematic drawings of lab test layout (Rollins and Jessee 2012) (NOTE 1 m = 3.281 ft).

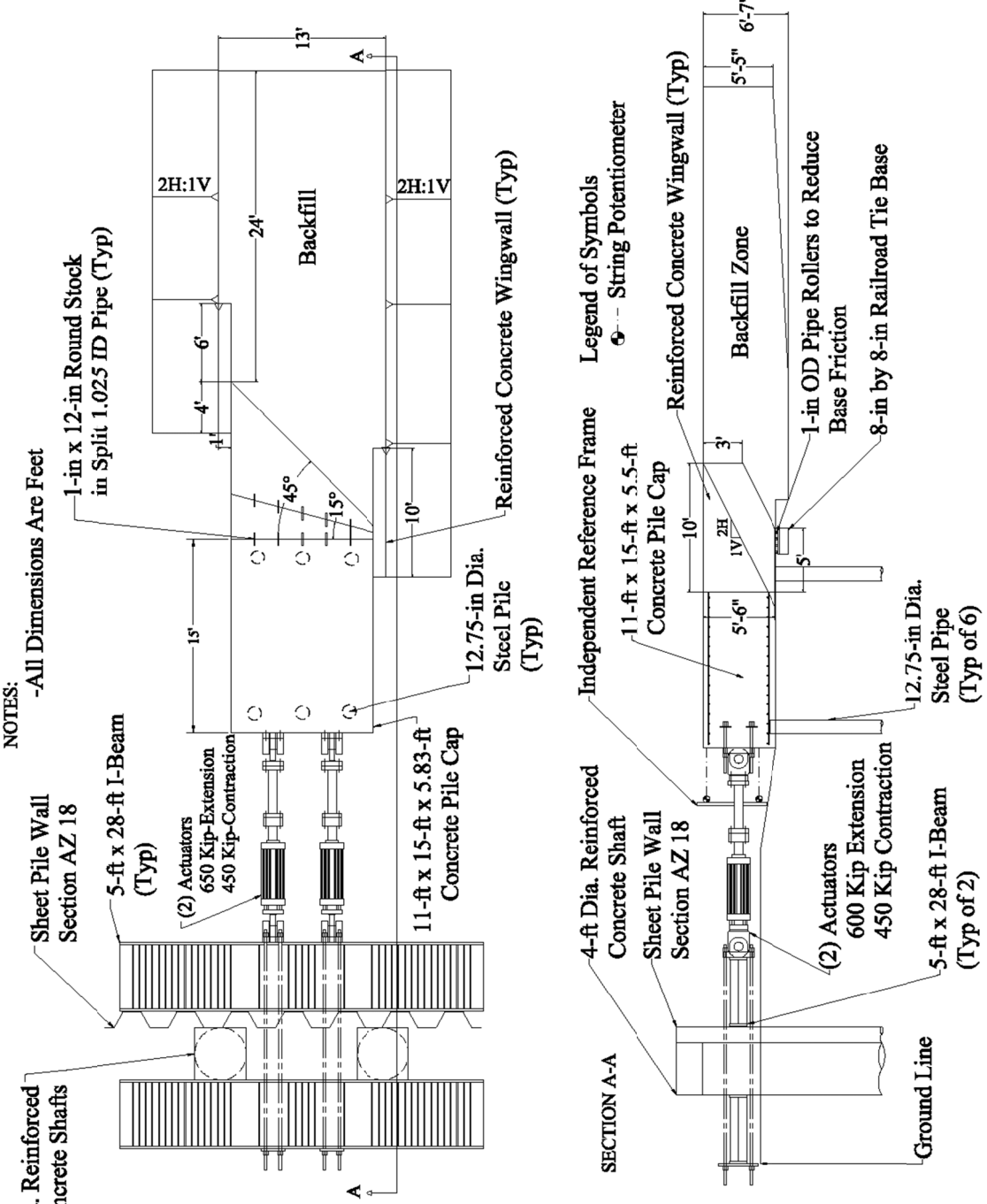

Figure 3. Schematic drawing of test configuration.

Wingwall reinforcment detail and concrete dimensions are illustrated in Figure 4. Although a true monolithic wingwall connection was not constructed for this test, that configuration was simulated by attaching precast reinforced concrete wingwalls to the existing pile cap using (10) ¾-in-diameter Redhead® wedge anchors embedded 7 inches into the pile cap. The bolted connection was designed to match the moment capacity of the steel reinforcement at the wingwall-pile cap interface from a typical wingwall design used by the Oregon Department of Transportation (ODOT). Wingwalls were attached to the west and east sides of the pile cap for both the 0º and 45º skew tests.

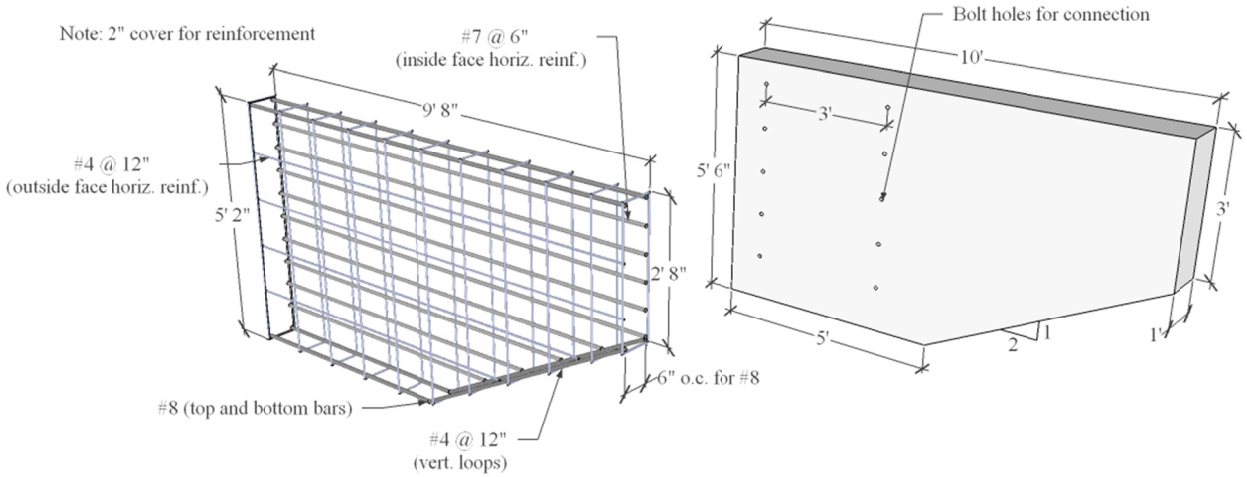

Figure 4. Wingwall reinforcement detail and concrete dimensions.

Instrumentation

Longitudinal load was measured using pressure transducers in the actuators. Six Geokon® pressure cells were installed along the face of the backwall for the 45° skew test only. Longitudinal displacement of the pile cap was measured using four string potentiometers located at each corner of the back of the pile cap that were tied to an independent reference frame. String potentiometers were also used to measure transverse displacement of the wingwalls. Shape accelerometer arrays recorded lateral deflection of the north and south center piles beneath the pile cap.

A grid of 2.0-ft (0.61-m) squares—refined to a grid of 1.0-ft (0.30-m) squares near the backwall for the non-skew test—was painted on the surface of the backfill. Vertical heave and horizontal

displacement of backfill were measured at grid intersections using a total station before and after both tests. Surface cracks in the backfill were marked in a field book during the tests as cracks daylighted. 2-in-diameter vertical holes were drilled with hand augers along 3 lines perpendicular to the face of the cap. These holes were then refilled and compacted with red-dyed sand forming a red column in the soil to help identify shear surfaces.

Strain gauges were attached to the reinforcement in the wingwalls at locations along the sides of selected No. 7 bars that were facing the backfill (see Figure 5). The strain gauges were instrumented in a vertical line pattern with 12 in spacing at 3 ft and 6 ft from the tapered end of the wingwalls. Two Geokon® pressure cells were embedded in the wingwalls; one at 2ft below the top and 2 ft in from the tapered end, and another 3 ft below the top and 4 ft in from the tapered end. A 3-dimensional view of the test setup and abutment geometry without the backfill is illustrated by the photo in Figure 6.

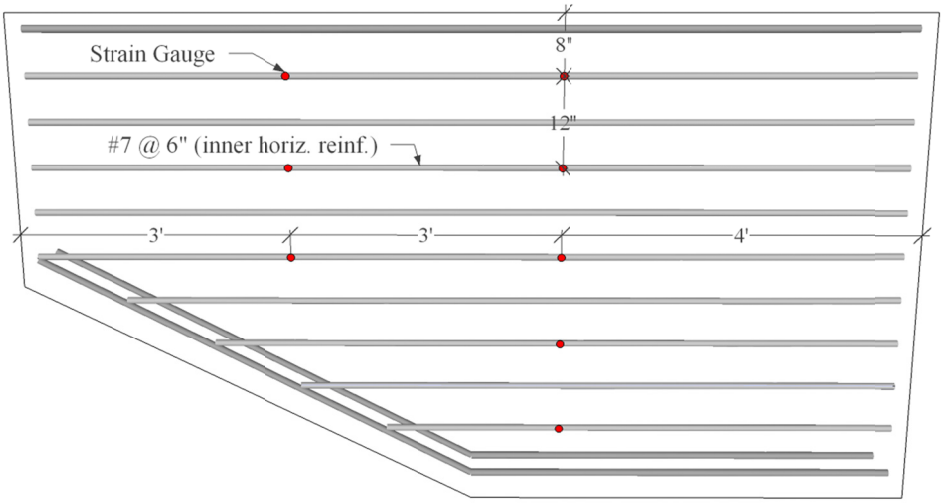

Figure 5. Strain gauge instrumentation on wingwall reinforcement.

Figure 6. Photo of test setup and abutment geometry for 45° skew test.

Geotechnical Backfill Properties

Backfill materials consisted of a poorly-graded sand (SP or A-1-b as classified by the Unified Soil Classification System or AASHTO classification system, respectively). The particle-size distribution curves generally fall within the gradation limits for washed concrete sand (ASTM C33) as shown in Figure 7. Gradation tests performed before and after a load test found that the coefficient of uniformity (C_u) and coefficient of curvature (C_c) were 7.6 and 0.8 pre-test, and 9.7 and 0.7 post-test, respectively. This variability is likely due to small differences in soil samples. For comparison, the C_u and C_c values from the lab tests were 3.7 and 0.7, respectively. Figure 7 also shows the soil gradation for the lab tests.

Unit Weight and Moisture Content

Maximum dry unit weight according to the modified Proctor compaction test (ASTM D1557) performed prior to testing was 111.5 lbf/ft^3 (17.52 kN/m^3) and the optimum moisture content was 7.1%.

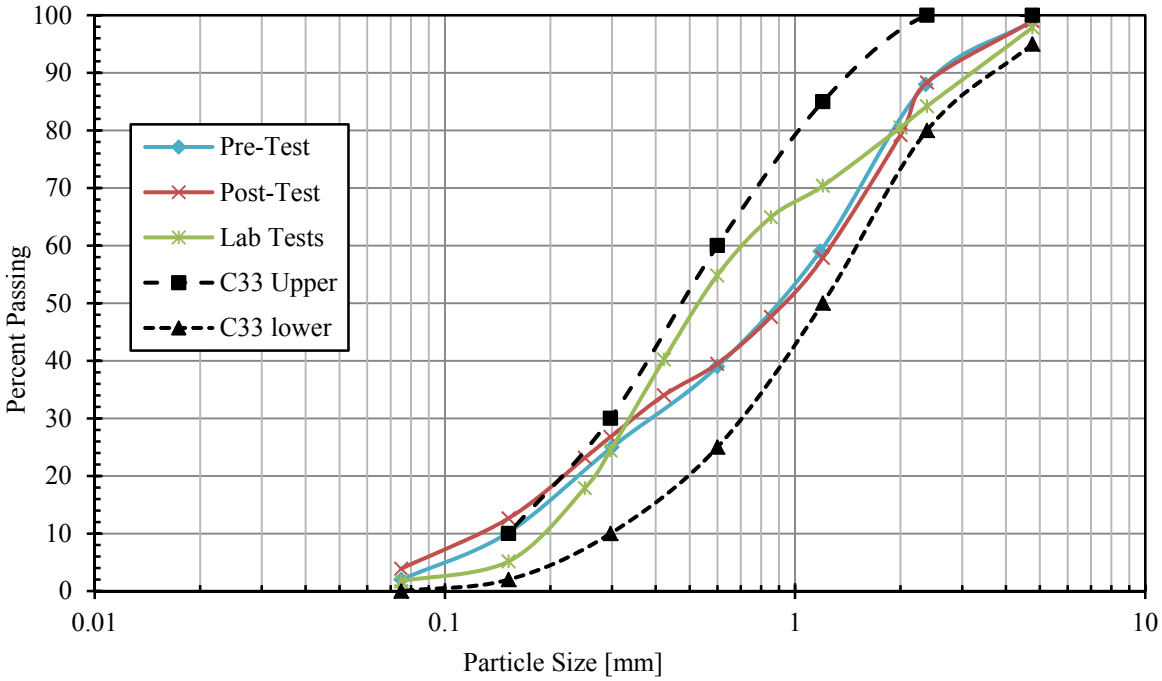

Figure 7 Gradation for backfill sand relative to concrete sand gradation.

The target on-site compaction level was 95% of the modified Proctor maximum or higher. Backfill sand was placed in lifts approximately 6-in (15.24-cm) thick and compacted with a smooth-drum vibratory roller and a walk-behind vibratory plate compactor to an average density greater than approximately 95% of the modified Proctor maximum. A nuclear density gauge was used to obtain relative compaction and water content data during compaction. Though not shown, the variation of relative compaction and moisture content with depth was not significant. Average relative density was estimated using the empirical relationship between relative density (D_r) and relative compaction (R) for granular materials developed by Lee and Singh (1971) as shown in Equation (7) where D_r and R are measured in percent.

$$R = 80 + 0.2D_r \quad (7)$$

A summary of the soil density and water content measurements for the three tests is shown in Table 1. The properties of the two backfills were generally very consistent. Average relative compaction, relative density, and water content for the two tests were 97.7%, 88.3%, 7.5%, respectively. For comparison purposes the average relative compaction, relative density, and water content for the laboratory tests were 97.9%, 90%, and 8.0%, respectively (Rollins and Jessee 2012).

Table 1. Summary of Compaction and Water Content Data for Each Test

Backfill Soil Properties	0° Skew Test	45° Skew Test	Average
Minimum Dry Unit Weight [pcf]	105.4	107.9	106.7
Maximum Dry Unit Weight [pcf]	109.9	112.9	111.4
Average Dry Unit Weight [pcf]	108.2	109.6	108.9
Relative Compaction	97.0%	98.3%	97.7%
Relative Density	85.0%	91.5%	88.3%
Moisture Content	7.2%	7.8%	7.5%

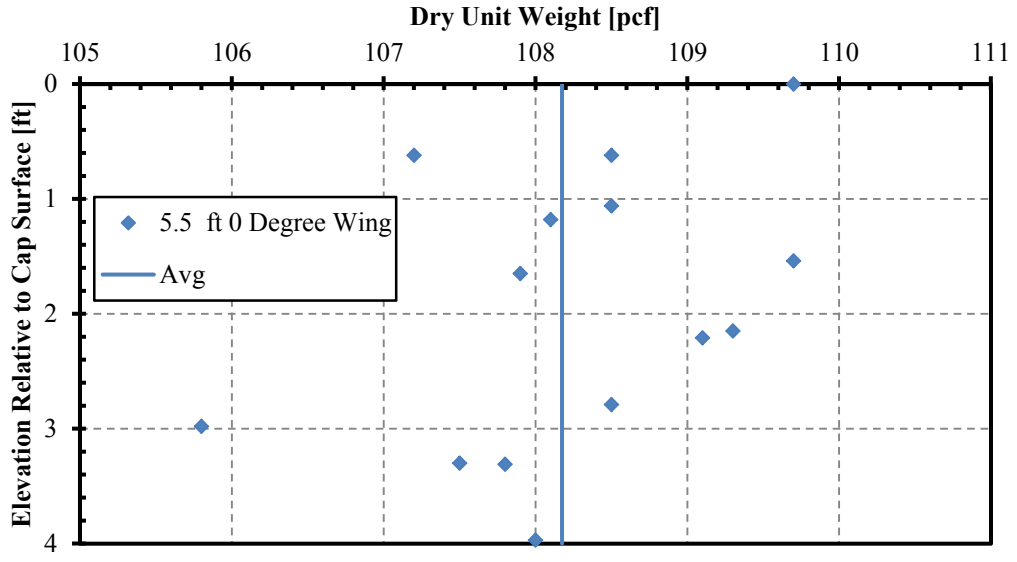

Figure 8. Dry unit weights for 0° skew.

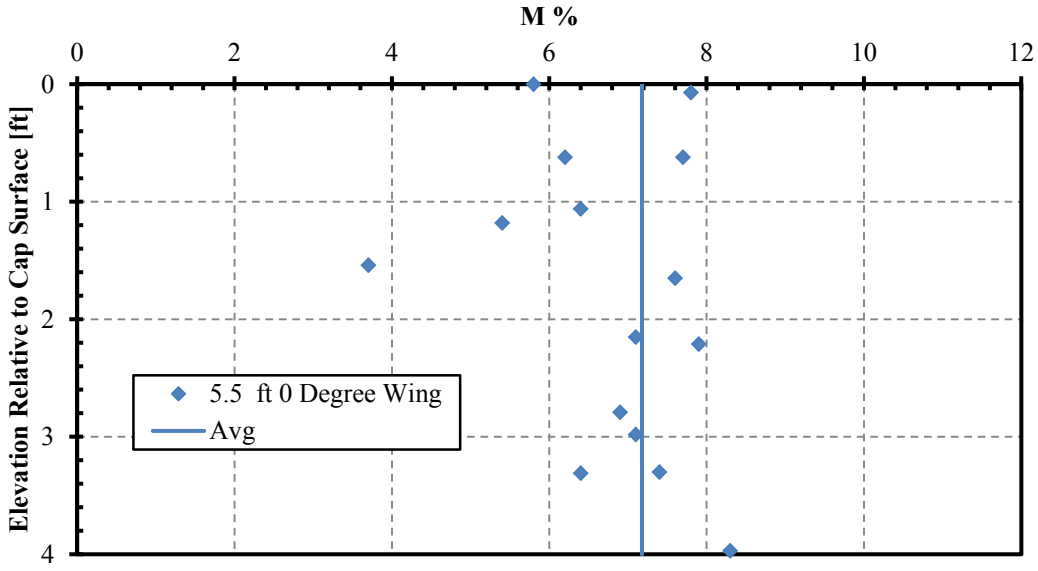

Figure 9. Moisture contents for 0° skew.

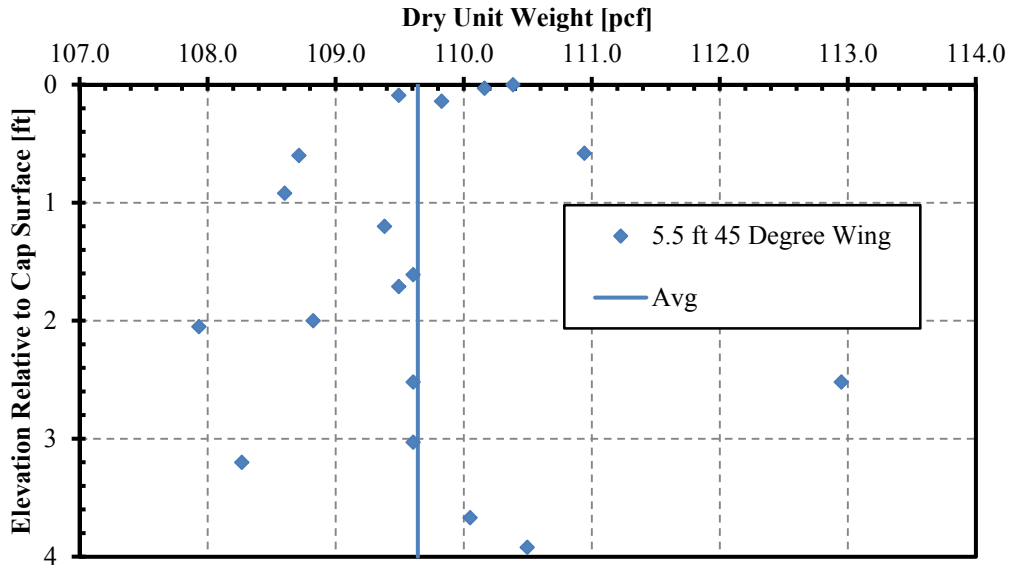

Figure 10. Dry unit weights for 45° skew.

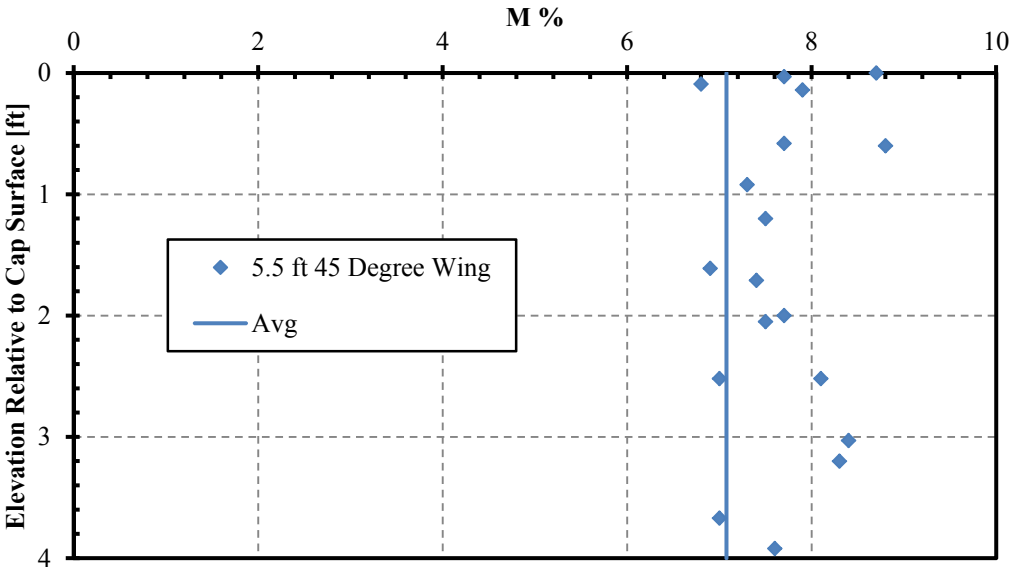

Figure 11. Moisture contents for 45° skew.

Shear Strength

Direct shear tests were conducted at the field density and moisture content values, and the drained friction angle (ϕ') was found to be 41° with a cohesion of 96 lbs/ft^2 (4.61 kN/m^2). Previous researchers (Rollins and Cole 2006; Rollins and Jessee 2012) conducted direct shear tests and determined that the

interface friction angle (δ) between similar sand and concrete was about 75% of the soil friction angle. For comparison purposes, the drained friction angle of the sand for the laboratory skew tests was 46° with a cohesion of 70 lbs/ft^2 (3.35 kPa) (Rollins and Jessee 2012).

General Test Procedures

Prior to testing with the backfill in place, a lateral load test was performed to determine the "baseline" resistance of the pile cap alone, and the pile cap with attached wedge. Because the pile cap had been previously employed for a number of tests, the baseline resistance has become relatively linear. Following the baseline test, backfill was compacted adjacent to the backwall, the grid and soil columns were installed, and appropriate initial measurements, including relative elevations and locations of the grid points, were recorded. The backfill material was completely excavated and re-compacted for each individual test.

Following initial measurements, a lateral load test was performed for both 0° and 45° skewed abutments where the pile cap and attached wingwalls were pushed longitudinally into the backfill in 0.25-in (6.35-mm) increments at a velocity of 0.05 in/min (6.35 mm/min) to a final displacement of approximately 3.0 in (7.62 cm) to 3.75 in (9.53 cm) using the two hydraulic actuators.

Plots of the total load and corresponding baseline curve for the non-skewed and 45° skewed test are shown in Figure 12 and Figure 13. The additional load of the 'total force' curve represents the resistance of the abutment backwall in the longitudinal direction, which is comprised of both the passive and shear resistance of the backfill against the backwall. Longitudinal resistance of the abutment backwall alone is found by subtracting the baseline curve from the total force curve.

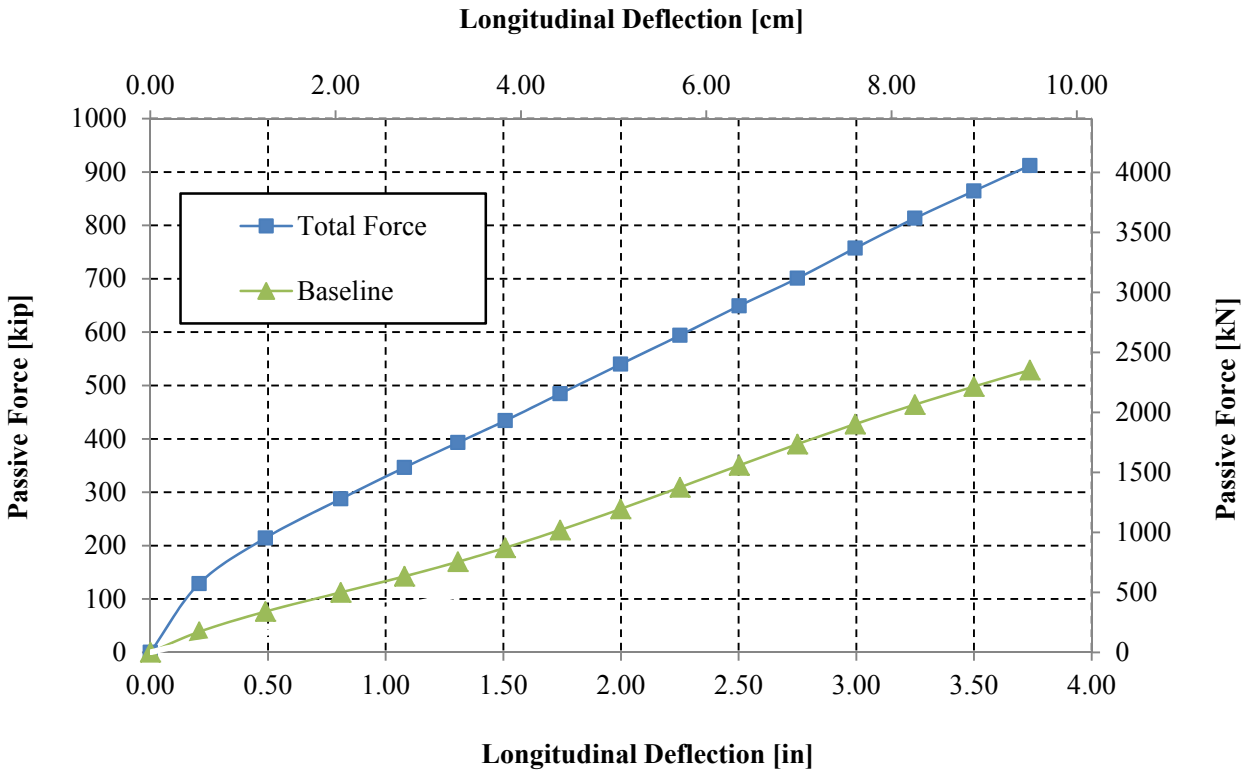

Figure 12. Total force and baseline resistance for 0° skew test.

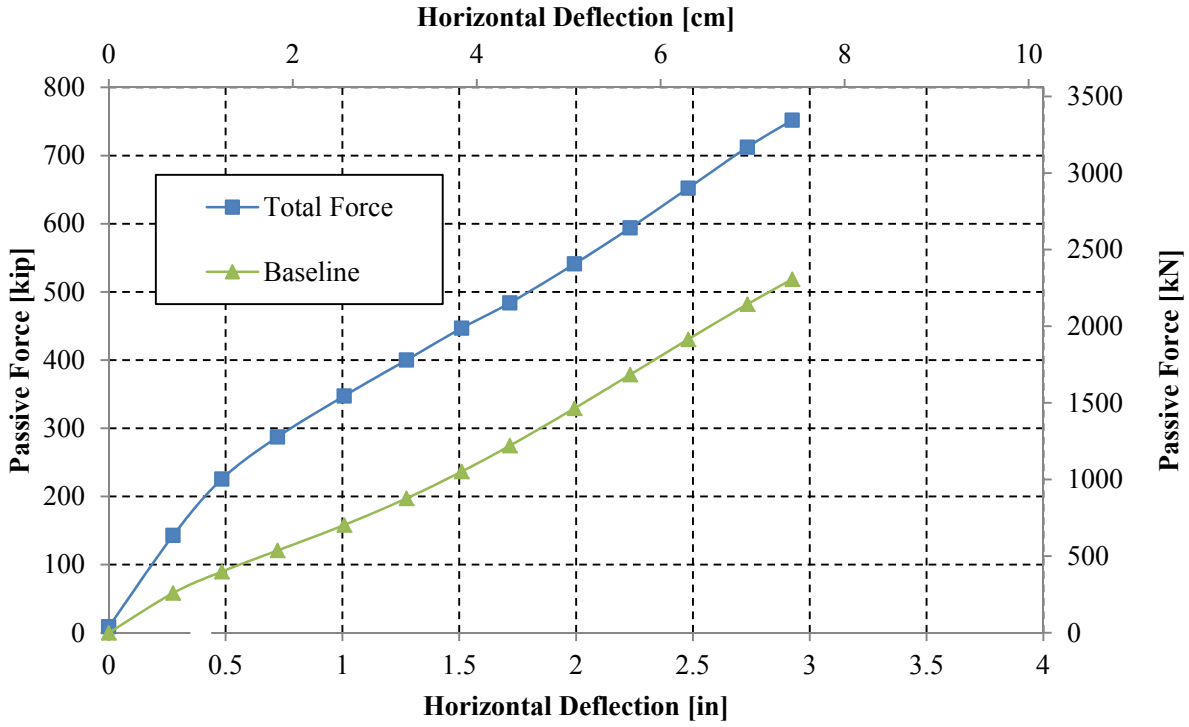

Figure 13. Total force and baseline resistance for 45° skew test.

TEST RESULTS

Passive Force-Deflection

Figure 14 shows the passive force versus longitudinal deflection curves for the 0° and 45° skew field tests. Passive force (P_P) was calculated using Equation (2), $P_P = P_L \cos\theta$, where the longitudinal load (P_L) was the actuator load corrected for the baseline curve.

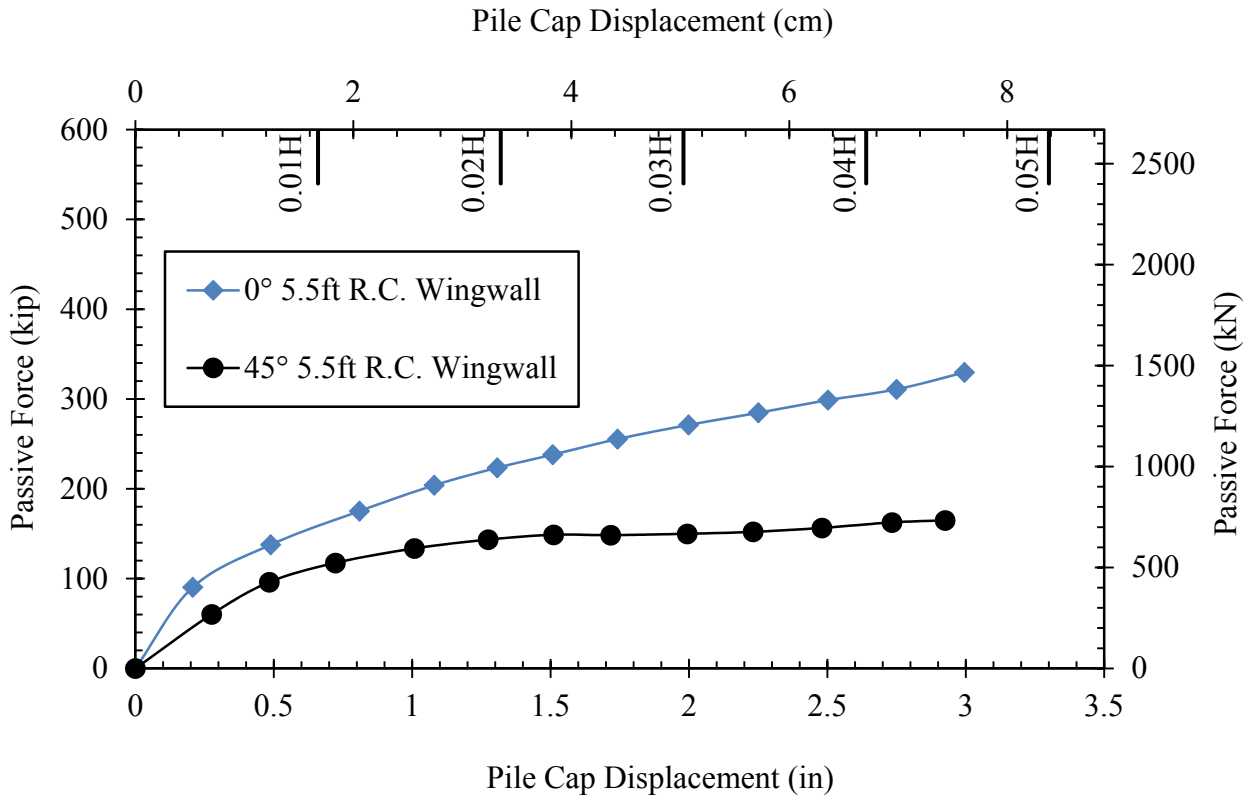

Figure 14. Passive force-deflection curves for 0° and 45° skewed abutments with reinforced concrete wingwalls.

Pile cap displacement was computed as the average deflection of the four string potentiometers on the back of the pile cap. Both 45° skewed and non-skewed abutments appeared to reach a peak passive force at approximately 3 in (7.62 cm), between 4% and 5% of the backwall height. The peak passive force for the 45° skewed abutment (≈165 kips) is approximately 50% of the peak passive force for the non-skewed abutment (≈330 kips). The 50% reduction in passive force for the 45° skewed abutment with reinforced concrete wingwalls is plotted in Figure 15 along with results from other tests and the proposed reduction curve by Rollins and Jessee (2012).

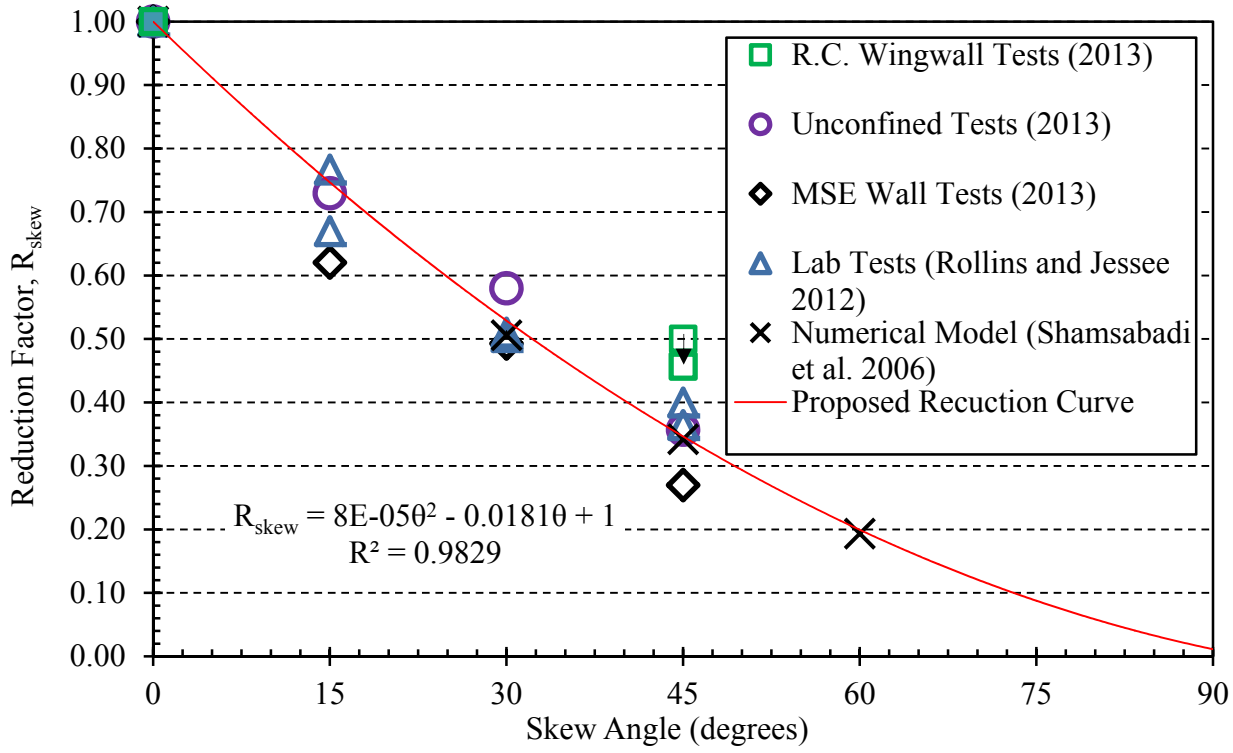

Figure 15. Reduction factor, R_{skew} (passive force for a given skew angle normalized to non-skewed passive force) plotted versus skew angle based on lab tests (Rollins and Jessee 2012), numerical analyses (Shamsabadi et al. 2006) and results from field tests in this study.

The reduction factor for the 45° skew reinforced concrete wingwall test is 15% above the recommended 35% reduction factor from the proposed reduction curve. This increased resistance may be partially explained by the increased frictional resistance from the wingwalls during the 45° test. Shape accelerometers observed 0.3 in (0.76 cm) of westward pile cap transverse deflection at 3.00 in (7.62 cm) of longitudinal displacement for the 45° test compared to 0.07 in (0.18 cm) of transverse deflection at 3.75 in (9.53 cm) longitudinal displacement for the 0° test. This increased transverse deflection for the 45° test suggests that the abutment-wingwall configuration slipped 0.3 in westward during northward longitudinal loading. The westward movement likely introduced additional normal passive force to the east wingwall, which subsequently increased the frictional resistance acting against the actuator loading.

Normal passive pressure from backfill on both wingwalls was measured for both tests and the increased frictional resistance on the east wingwall for the 45° test was computed using Equation (8)

$$Friction = N * tan\delta \text{ ,} \tag{8}$$

where

$$N = Normal\ force\ acting\ on\ wingwall \tag{9}$$

$$\delta = 0.75\varphi, \qquad where \tag{10}$$

$$\varphi = soil\ friction\ angle \tag{11}$$

$$\delta = wall\ friction\ angle \tag{12}$$

Subtracting the increased frictional resistance from the 45° test lowers the resistance to an R_{skew} value closer to the proposed reduction curve, represented in Figure 15 by the downward arrow and additional point for R.C. Wingwall Tests (2013).

Pile Cap Displacement vs. Depth

Figure 16 and Figure 17 provide longitudinal deflection versus depth profiles obtained from both an inclinometer and a shape accelerometer array (SAA) for the 0º and 45° skew tests. Both profiles represent pile cap behavior for the final longitudinal displacement of the test. The depths are referenced to the top of the cap. The average deflection measured by the string pots at two elevations on the pile cap are also shown for comparison purposes. The graphs demonstrate that the measurements for the three systems were reasonably accurate and aligned with each other. The percent difference between the inclinometer and shape array profiles from the top of the cap to a depth of 15 ft (4.6 m) ranges between 0.3 and 7.0% with an average of 2.5% for the 0° skew test and 0.2% and 4.6% with an average of 1.9% for the 45° skew. The displacements below a depth of 15 ft (4.6 m) are very small and the error values in this zone are less than 0.02 inch and not particularly meaningful. Similar good agreement was obtained between the shape array and inclinometer for the other tests.

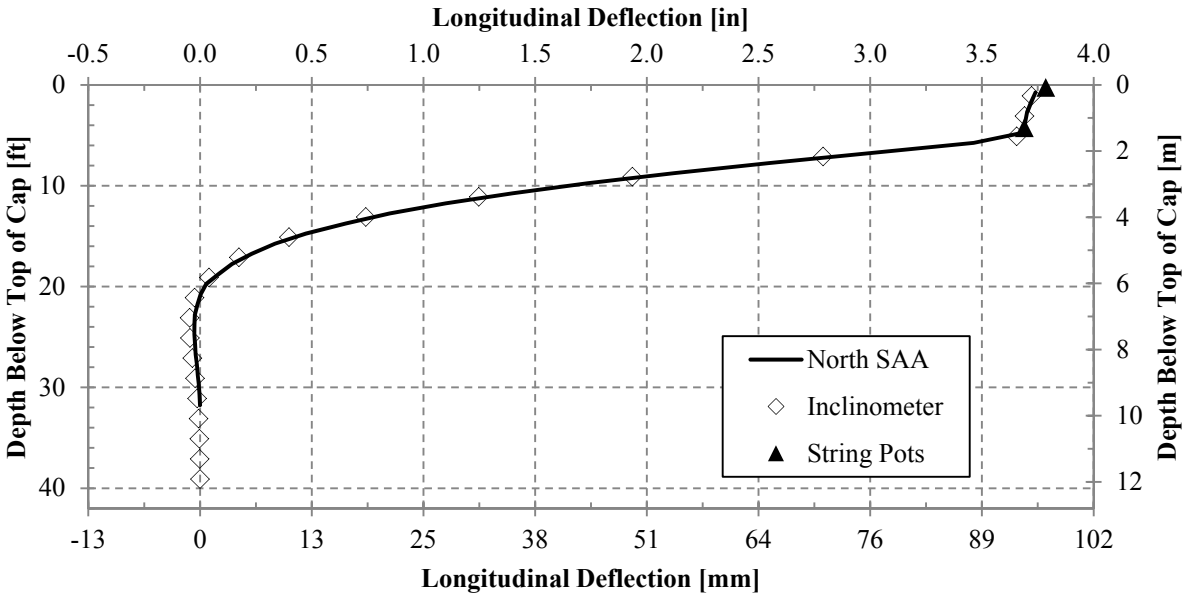

Figure 16. North 5.5-ft backfill 0° skew final longitudinal deflection; comparing inclinometer, shape array, and string potentiometers.

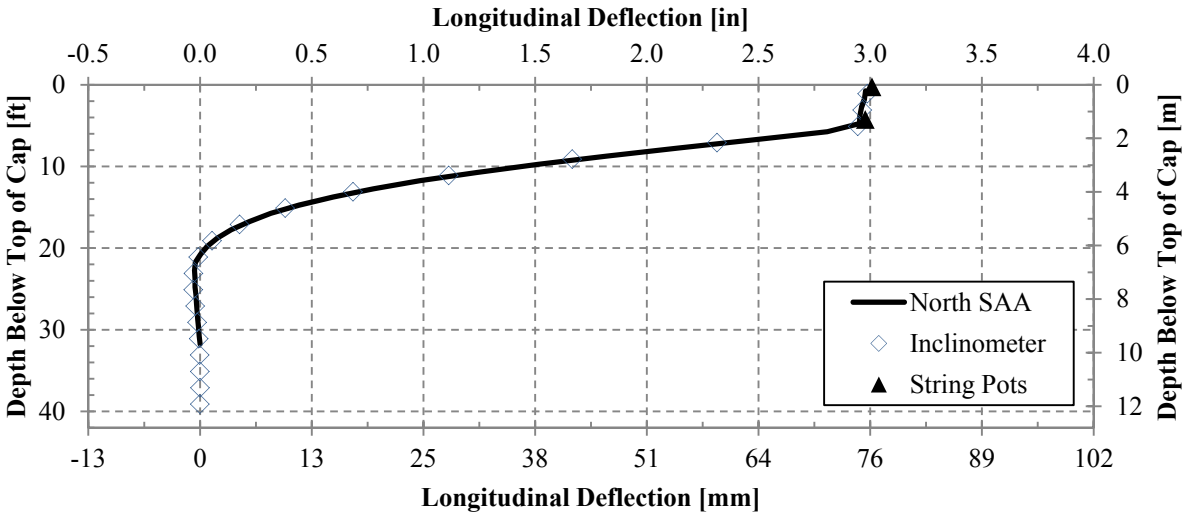

Figure 17. North 5.5-ft backfill 45° skew final longitudinal deflection; comparing inclinometer, shape array, and string potentiometers.

The measurements indicate a relatively linear deflection profile within the pile cap and small cap rotations. Below the base of the cap, the piles deflect in a non-linear fashion with the deflections reaching a point of counterflexture at depth of approximately 21 ft (6.3 m) and a point of fixity at about 31 ft (9.45 m). Agreement between the north and south inclinometers was generally very good.

Transverse deflection versus depth profiles for the pile cap, recorded by shape array and inclinometer, are also plotted in Figure 18 and Figure 19. Plotted on a smaller scale, the percent error seems larger than the longitudinal error although the magnitude difference is small. As observed for the deflections below 20 ft (6 m) in the longitudinal test, the percent difference is also exaggerated due to the smaller scale. The percent difference is within the error thresholds of each instrument ($\pm$1.5 mm/30 m for shape array, and $\pm$1.24 mm/30m for inclinometer). Once again, the shape of the deflection profile indicates essentially linear deflection in the pile cap and very small rotations. The deflection in the piles is non-linear and decreases to zero at a deflection of about 20 ft (6 m).

Although the inclinometer readings were only taken at the maximum deflection for each load test, shape array profiles in the longitudinal and transverse directions were obtained at each deflection increment for each test. For example, Figure 20 and Figure 21 show profiles of longitudinal deflection vs. depth for each deflection increment for the 0° and 45° skew tests. Similar curves were obtained in the transverse direction. As the deflection level increases the deflection of the pile cap remains linear but the rotation progressively increases while the depth to the point of fixity increases. At smaller deflection levels there are some variations associated with the small measurement errors; however at larger deflections, the data was accurate and useful in visualizing the pile movement.

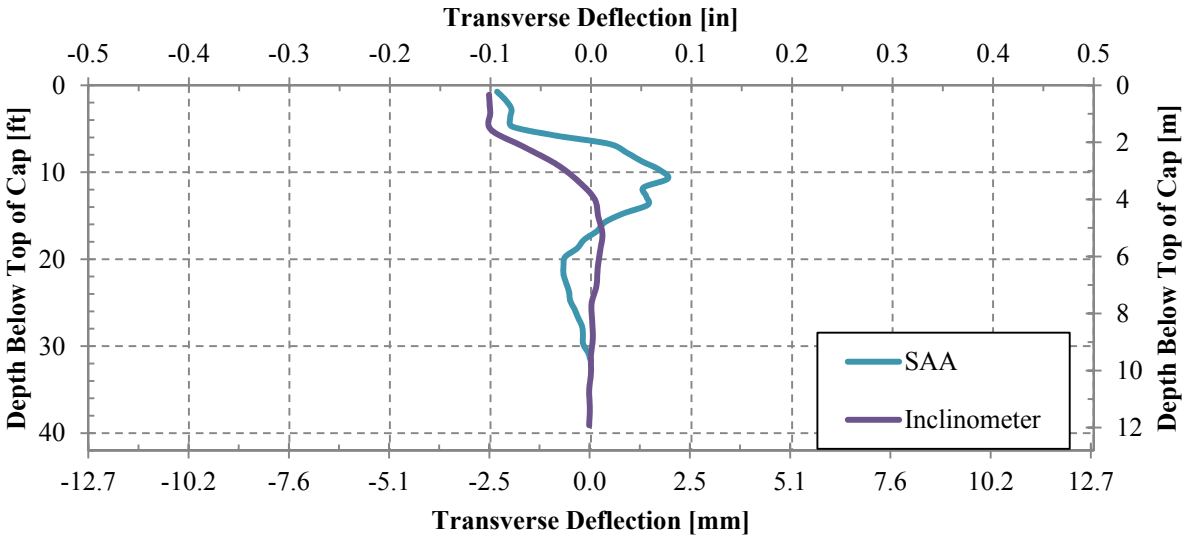

Figure 18. North 5.5-ft backfill 0° skew final transverse deflections; comparing inclinometer and shape array.

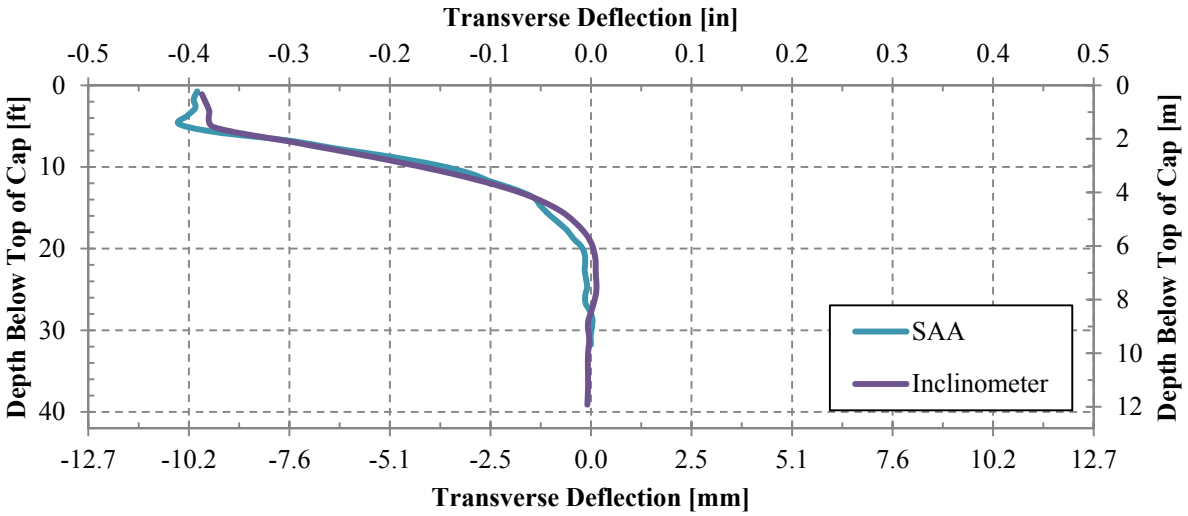

Figure 19. North 5.5-ft backfill 45° skew final transverse deflections; comparing inclinometer and shape array.

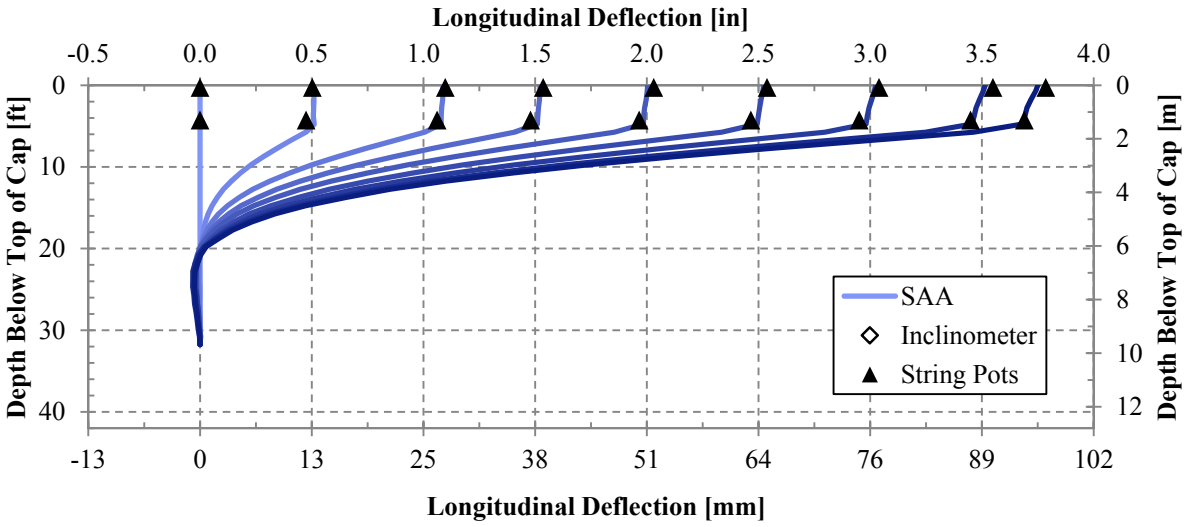

Figure 20. North longitudinal deflection vs. depth curves from shape array, inclinometer, and string potentiometer data at various deflection increments for 0° skew reinforced concrete wingwall test.

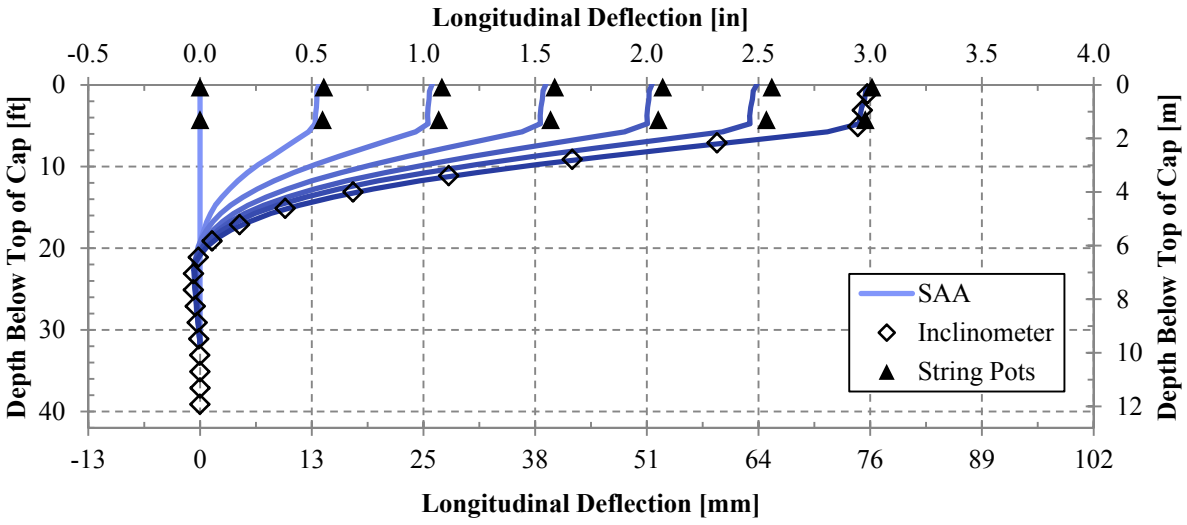

Figure 21. North longitudinal deflection vs. depth curves from shape array, inclinometer, and string potentiometer data at various deflection increments for 45° skew reinforced concrete wingwall test.

As noted previously, the inclinometer and shape arrays measured transverse deflections for the north and south sides of the pile cap with depth. The measured transverse deflections at the top of pile cap on both the north and south sides of the cap after the last deflection increment for each test are plotted in Figure 22 from a plan view perspective. By connecting these points on the north and south sides, the rotation of the cap can be visualized. Although deflections of both actuators were kept relatively constant throughout the test, rotation and transverse deflection were still affected by the skew angle in the 45° skew test. As seen in Figure 22, for both the 0° and 45° skews the pile cap ultimately shifted to the left (the direction of the skew) by approximately 0.09 and 0.34 inch, respectively and rotated counterclockwise approximately 0.01° and 0.04°, respectively. The shape arrays match the inclinometers almost exactly in Figure 22 because transverse deflection was the parameter used to calibrate SAA orientation.

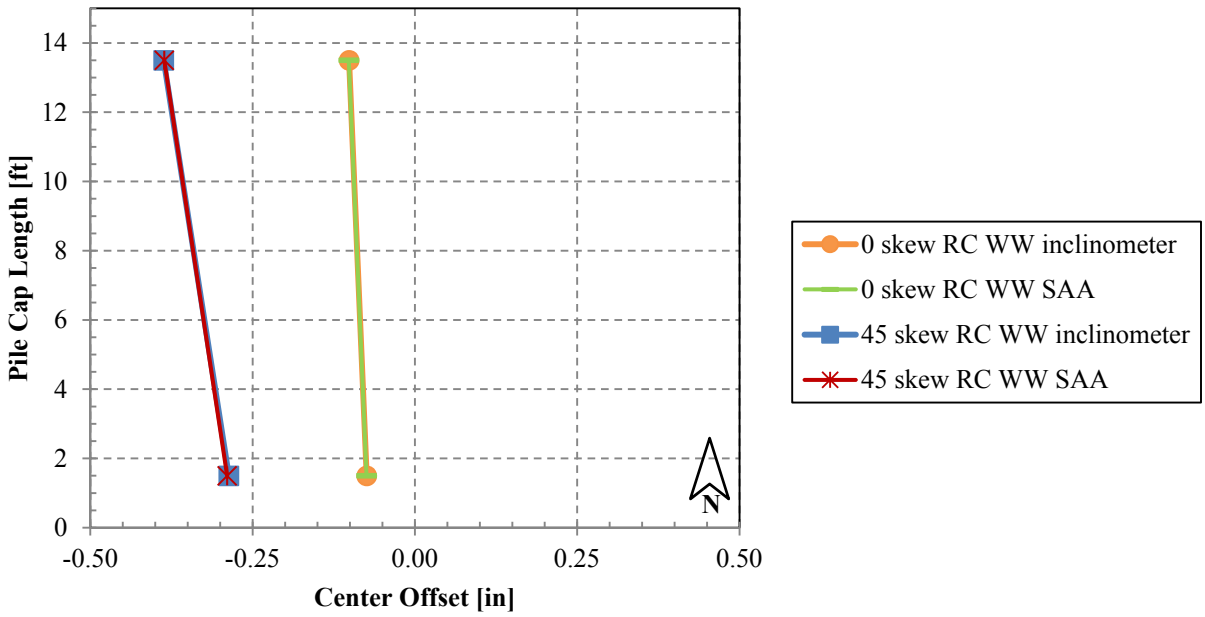

Figure 22. Transverse pile cap deflection and rotation determined between north and south shape array and inclinometer data.

Pressure Distribution

Figure 23 shows the lateral pressure readings along the abutment backwall from the pressure plates. The pressure plates show a pressure pattern similar to that observed in previous large scale tests conducted in this study. The pressure is generally lowest near the center of the wall and pressure increases at the outside edges of the wall. Measurements indicate that pressure was slightly higher at the acute end of the abutment relative to the obtuse side. Beyond a deflection of 2.5 inches the pressure remain relatively consistent across the width of the cap. Any additional load provided by the soil must be occurring elsewhere, possibly along the front edge of the wingwalls, at a different depth along the backwall, or by mobilizing frictional resistance along the longitudinal face of the wingwalls.

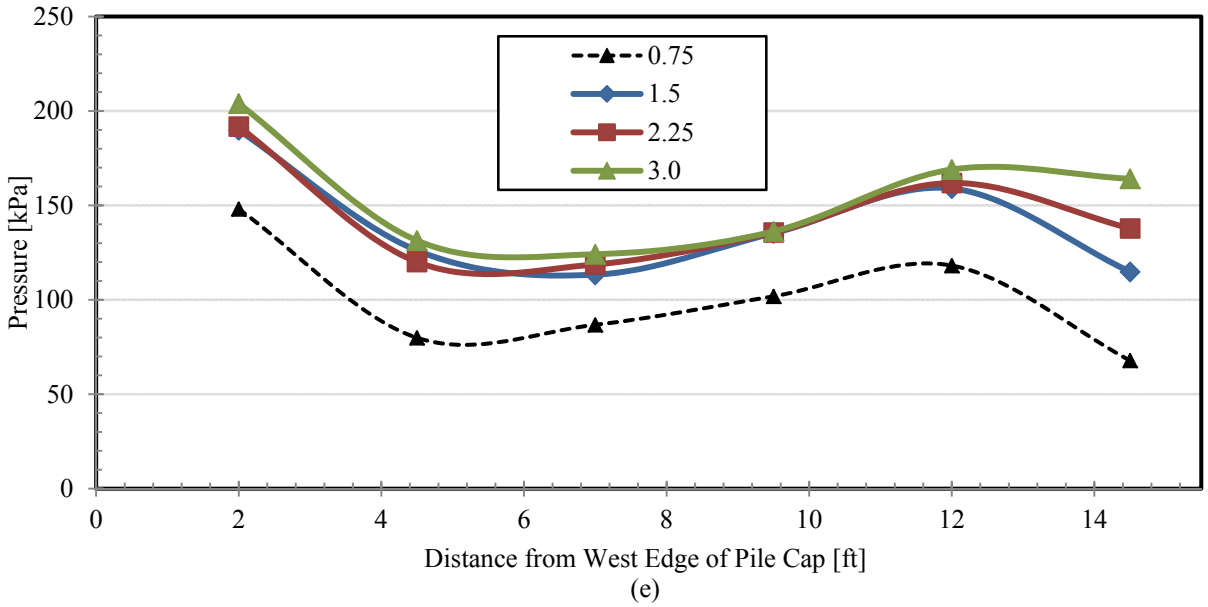

Figure 23. Pressure Distribution vs. Displacement for 45° skew test.

Figure 24 shows a comparison of the passive force derived from the pressure plates (at a depth of 44.5 inches below the top of the backwall) and the passive force measured by the actuators. The pressure plate readings assume no cohesion and thus presume a triangular pressure distribution vertically along the wall. To obtain a passive force from the pressure plate data, the initial readings were corrected for temperature, multiplied by 0.75 in order to find the average pressure along the height of the wall, then

multiplied by their respective tributary areas and summed. Although the shape of the passive force-deflection curve follows the trend obtained from the actuator, the computed passive force is 20% to 30% higher measured by the actuators. Nevertheless, these results suggest that the patterns of pressure measured by the pressure plates are reasonable.

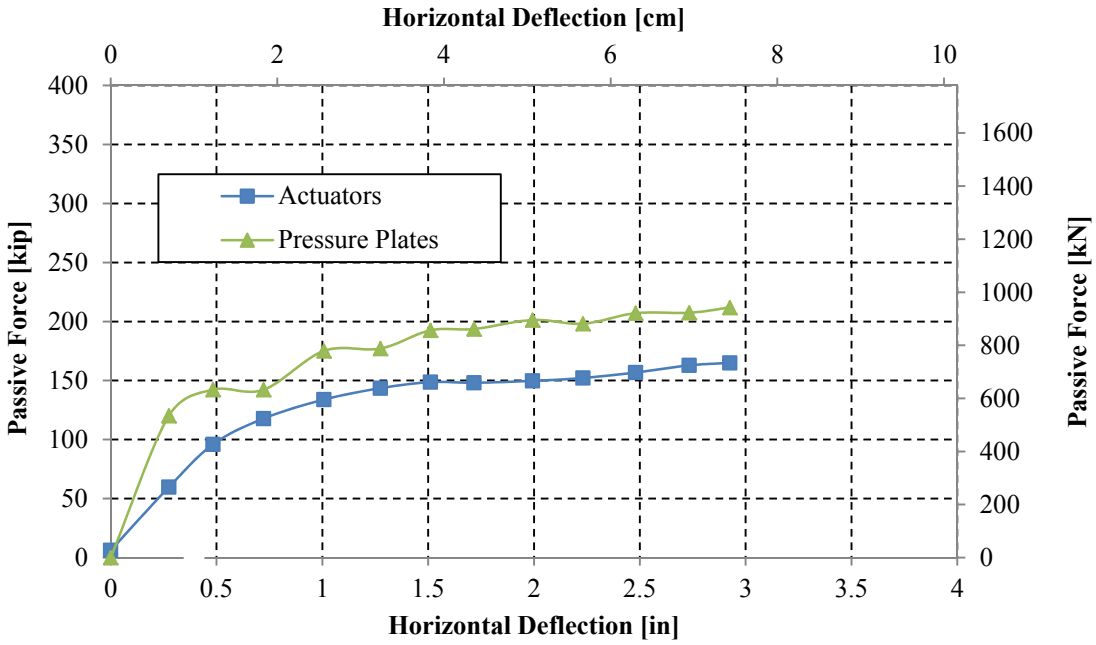

Figure 24. Comparison of force measured by actuators and Geokon® pressure cells for 45° skewed abutment.

Backfill Response

The direction and magnitude of horizontal backfill displacement is illustrated in Figure 25 for both tests. For the non-skewed test, the backfill appeared to displace generally parallel to the loading direction, with an average direction of 87° measured counterclockwise from the pile cap face. For the 45° skewed test, the average direction of backfill displacement was 101°, indicating more westward movement of the backfill when compared to the non-skewed backfill displacement. The westward movement of the backfill for the 45° skewed test is in good agreement with the larger westward transverse deflection of the entire abutment. Displacement vectors from the non-skewed test suggest that the soil confined within the wingwalls generally moved as one mass. For the 45° skewed test, the highest level of confinement was in the corner between east wingwall and the abutment backwall, which is where

the largest backfill displacements occurred. These larger displacements at the corner between the east wingwall and abutment wall agree with the larger normal forces that developed on the east wingwall in the 45° skewed abutment compared to the non-skewed abutment, which would lead to increased frictional resistance along the east wingwall. The lack of confinement from the wingwalls in the 45° skewed test seemed to allow the soil to displace more freely when compared to the non-skewed test.

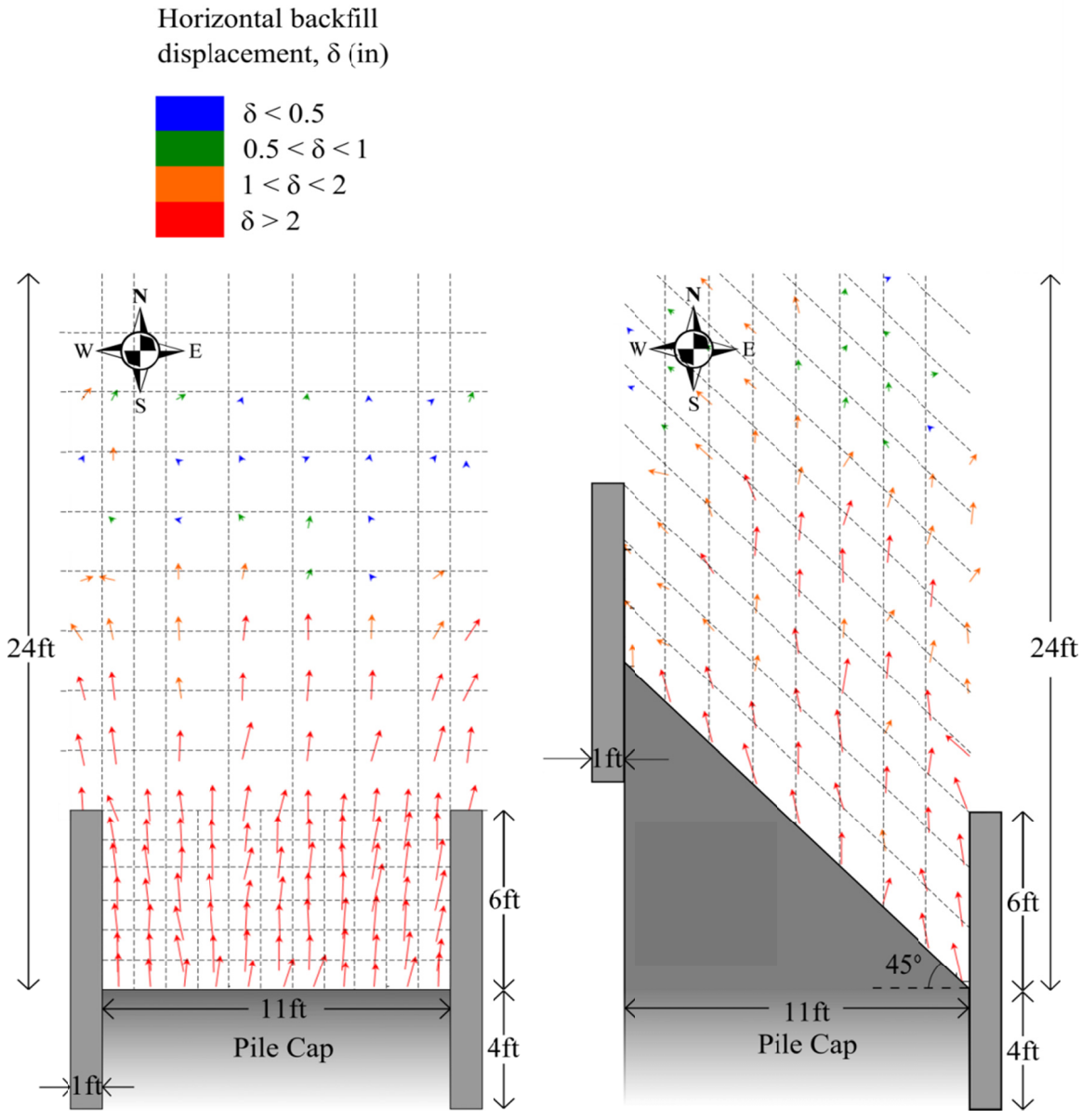

Figure 25. Horizontal backfill displacement for 0° and 45° skew at test completion (2ft grid in vertical direction and parallel to abutment skew—refined to 1ft grid within 6ft of pile cap for 0° skew test).

Backfill vertical heave contours are illustrated in Figure 26. The maximum heave for the non-skewed test was 2.3 in (5.8 cm) at about four feet out from the center of the pile cap face, which was approximately 3.5% of the backwall height. Surface cracks extended outward from the edge of both wingwalls and converged at a central point approximately 15 ft out from center of the pile cap face. Maximum heave for the 45° skewed test was only 1.4 in (3.6 cm), 2.1% of the backwall height, located about 6 ft longitudinally outward from the abutment wall face. Long surface cracks, which formed during cyclic loading before the abutment was deflected 3 in into backfill, daylighted within 4 ft of the abutment wall and were roughly parallel to abutment wall.

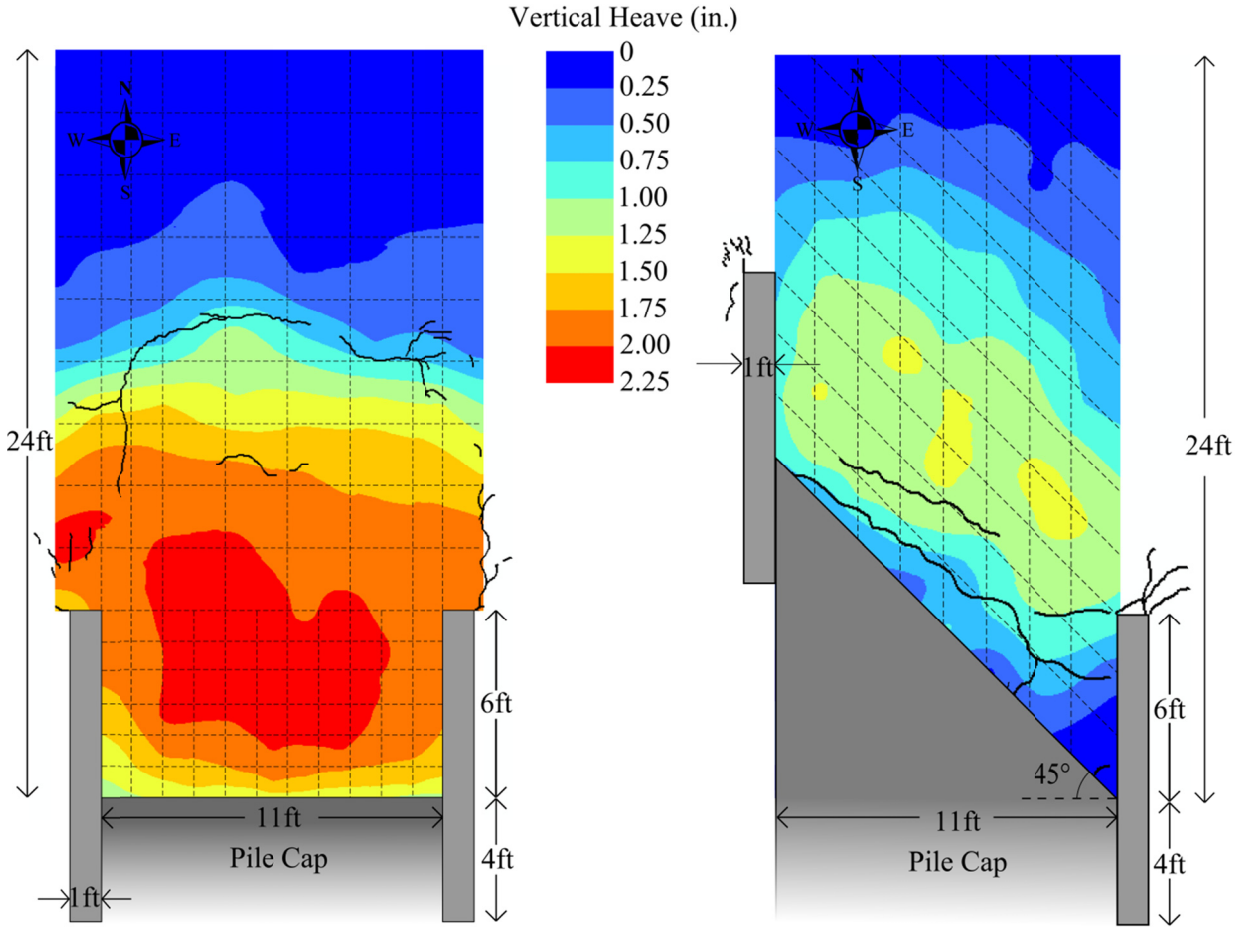

Figure 26. Heave contours and surface cracks for 0° and 45° skew at test completion (2ft grid in vertical direction and parallel to abutment skew—refined to 1ft grid within 6ft of pile cap for 0° skew test).

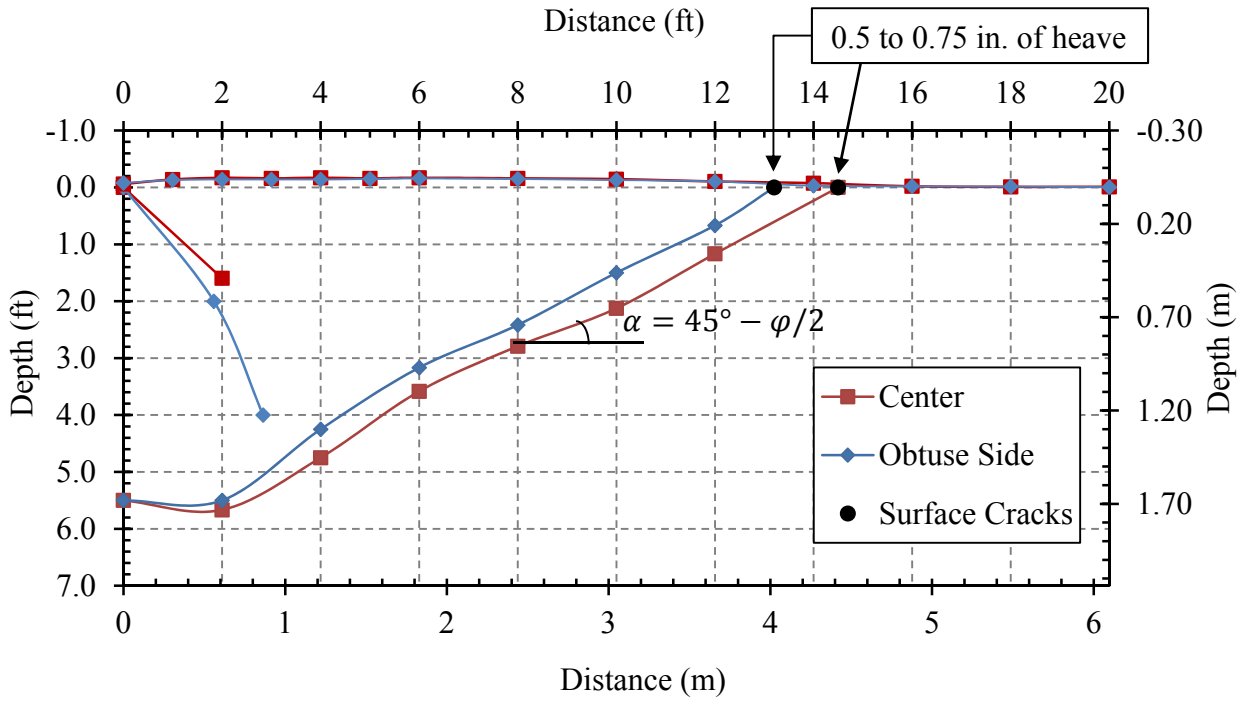

Figure 27. East and west shear planes and ground surface heave geometries for 0° wingwall skew test; inset shows plan view with approximate locations of red soil columns.

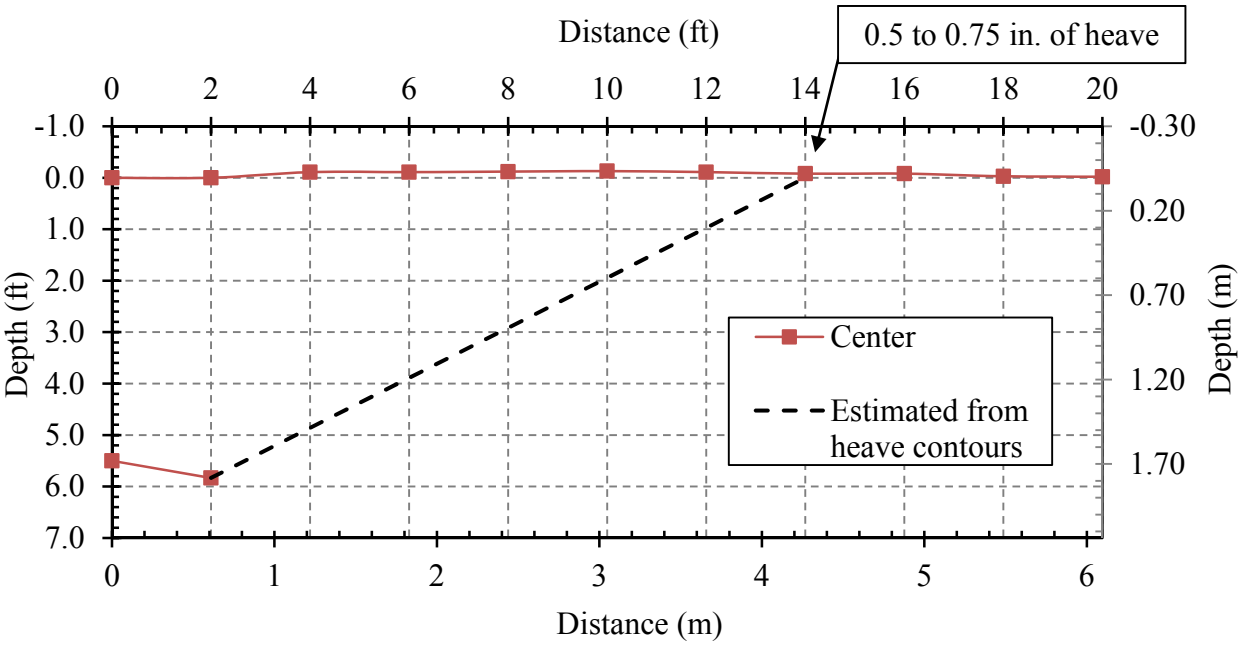

Figure 28. Shear plane geometry and ground surface heave for 45° wingwall skew test (estimated failure line based on recorded heave measurements).

Figure 27 and Figure 28 show the location of the failure planes behind the non-skewed and 45° skewed abutments. The failure surfaces show a log spiral portion followed by a linear Rankine failure wedge. Based on heave patterns, the failure surface for the 45° test would have likely daylighted around 14ft longitudinally from the face of the wedge; however, no clear failure crack was observed. In the 0° skew test, the failure surface daylighted at about 15ft longitudinally from the face of the wedge. Results from RC wingwall tests are consistent with previous large scale tests, which indicate that passive failure surfaces tend to daylight at heave values between 0.5 and 0.75 inches.

The average angle of inclination of the linear portion of the failure surfaces for the 0° skew test was 25°. Assuming the relationship between friction angle and the angle of inclination (α) of the failure surface shown in Equation (13), the approximate friction angle for the 0° skew tests would be 40°. This value is reasonably consistent with the friction angle determined by the direct shear test.

$$\alpha = 45 - \phi'/2 \tag{13}$$

The 45° test showed an angle of inclination of roughly 30°. This leads to a friction angle of roughly 34°.

Detailed profile views of backfill heave measurements for both tests are shown in Figure 29 and Figure 30. The heaved zone for the 0° skew test is clearly associated with the failure mass and decreases to about 0 when the failure surface daylights. Based on the heave pattern the failure surface in the 45° skew would be expected to daylight at about 18 ft. In both cases, the maximum heave does not occur at the wall face, but develops some distance back from the wall face.

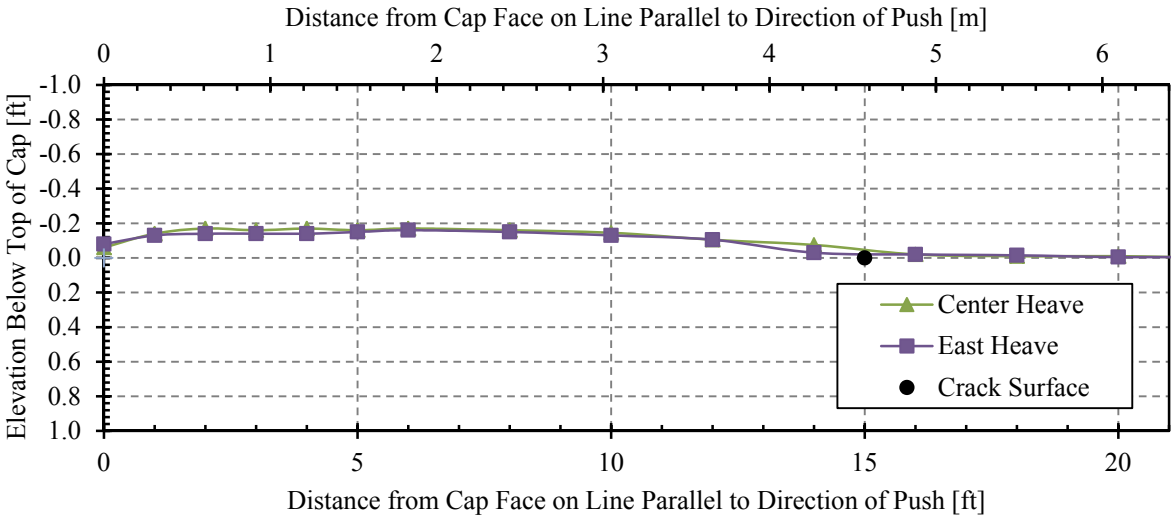

Figure 29. East and West Ground surface heave geometries for 0° wingwall skew test; inset shows plan view with approximate locations of red soil columns.

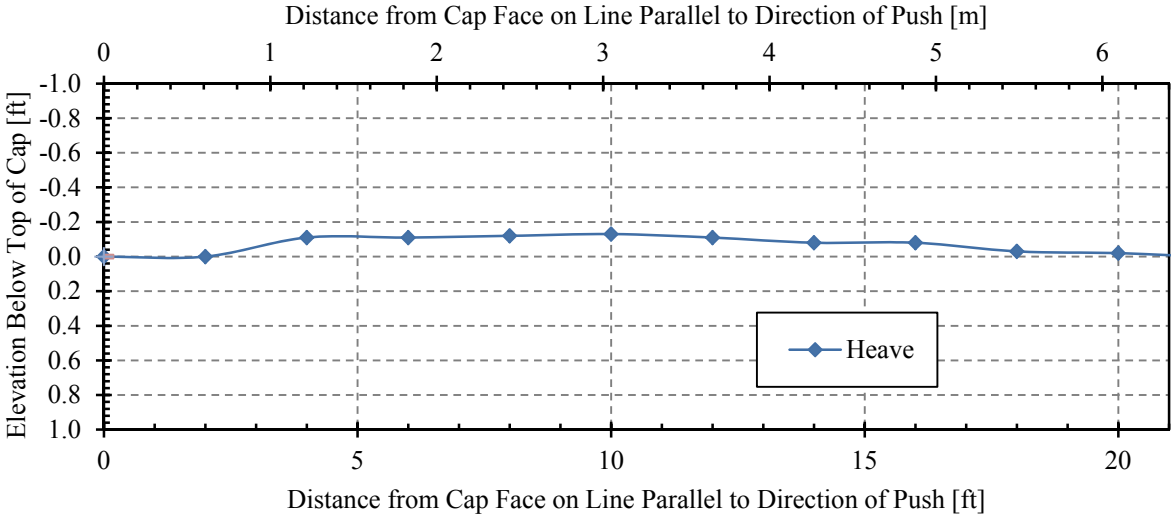

Figure 30. Ground surface heave for 45° wingwall skew test (estimated failure line based on recorded heave measurements).

Structural Response of Wingwalls

Moment distributions were calculated from strain gauges instrumented on wingwall reinforcement at 3ft and 6 ft from the tapered end. The moment distributions at the maximum deflection

for both tests are shown in Figure 31. Strain gauges instrumented 6 ft from the tapered end are roughly in line with the pile cap face. Based on the strain gauge readings, relatively small moments developed in the wingwall reinforcement on the non-skewed abutment, although moments were generally larger near the pile cap. A noticeable increase in moment was developed on the east wingwall reinforcement in line with the pile cap on the 45° skewed abutment, which is in good agreement with backfill displacement results. In general, maximum moments occurred 20 in below the top of the wingwall, which is about the midpoint of the 3-ft tapered end. The depth of the maximum moment appears to be caused by the upward taper of the wingwall.

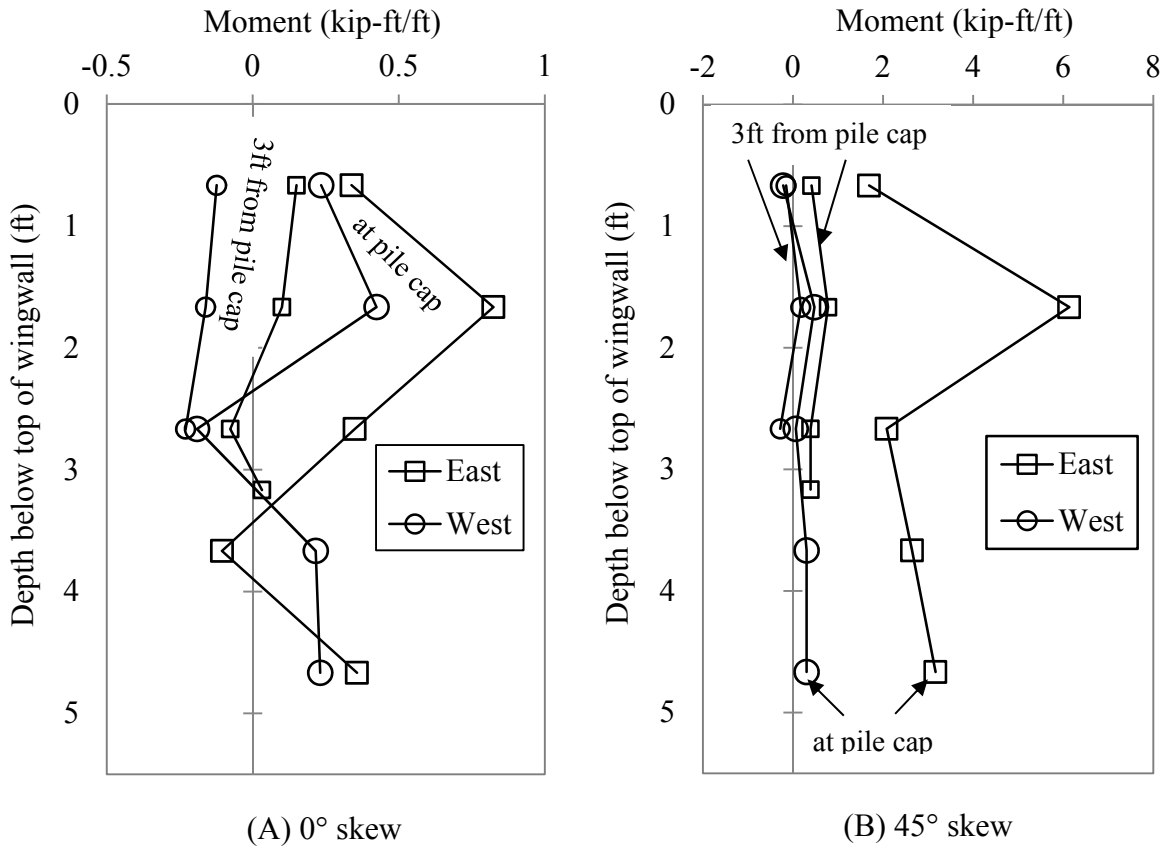

Figure 31. Moment distributions in wingwalls at test completion: (A) 0° skew. (B) 45° skew.

Transverse wingwall deflections were measured with string potentiometers and deflections at the maximum longitudinal deflection are illustrated in Figure 32. Wingwalls on the non-skewed abutment appear to bulge outward with the 3-D soil shear plane. Maximum transverse wingwall deflection for the non-skewed abutment was measured on the tapered end of the west wingwall and was approximately 0.3 in (0.76 cm).

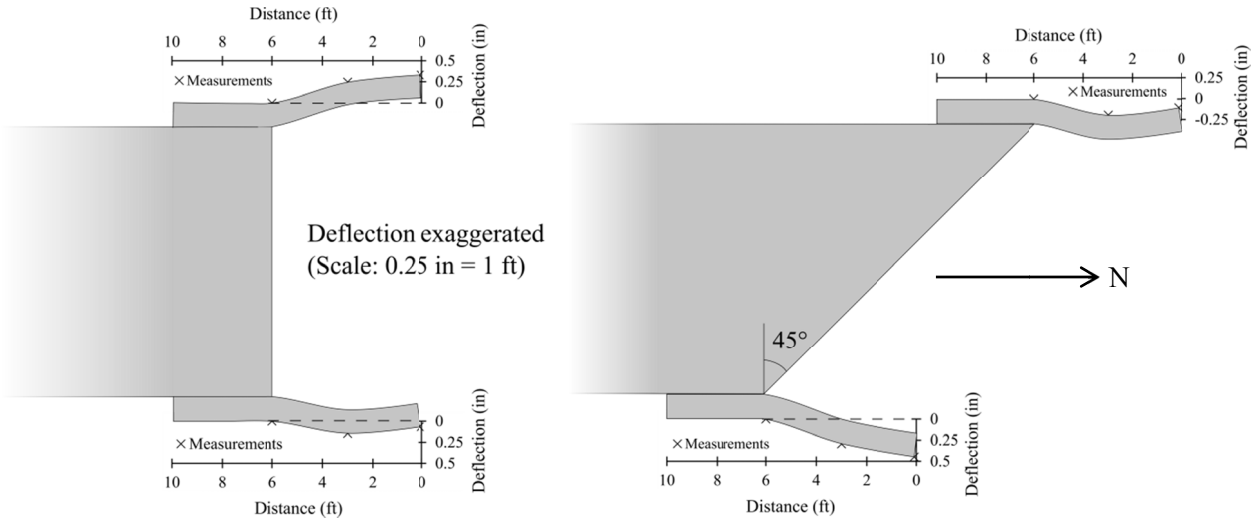

Figure 32. Transverse wingwall deflection at test completion for 0° and 45° skew test.

Wingwall deflection for the 45° skewed abutment reflects the westward movement of the abutment during lateral loading. Both wingwalls deflected in the same general direction, which seemed to be in response to being forced into the soil on the west side of both wingwalls. Maximum wingwall deflection was approximately 0.5 in (1.27 cm) and was measured at the tapered end of east wingwall. Larger deflections on the 45° skewed abutment east wingwall were expected after development of moment distributions.

Geotechnical Response of Wingwalls

Horizontal soil pressure distributions with depth along wingwalls were back-calculated from the moment distributions and are shown in Figure 33. The soil pressure distributions from Figure 33 exhibit very similar patterns to soil pressure distributions developed by Bozorgzadeh et al. (2008) at the

University of California, San Diego who performed lateral load tests on a non-skewed test abutment with reinforced concrete wingwalls in a silty sand backfill. Bozorgzadeh et al. (2008) plotted soil pressure versus depth at the west side and center of the test abutment (see Figure 34). Although soil pressure was measured on the abutment wall (not on wingwalls), the pressure distribution shape closely resembles those for the wingwalls in this study.

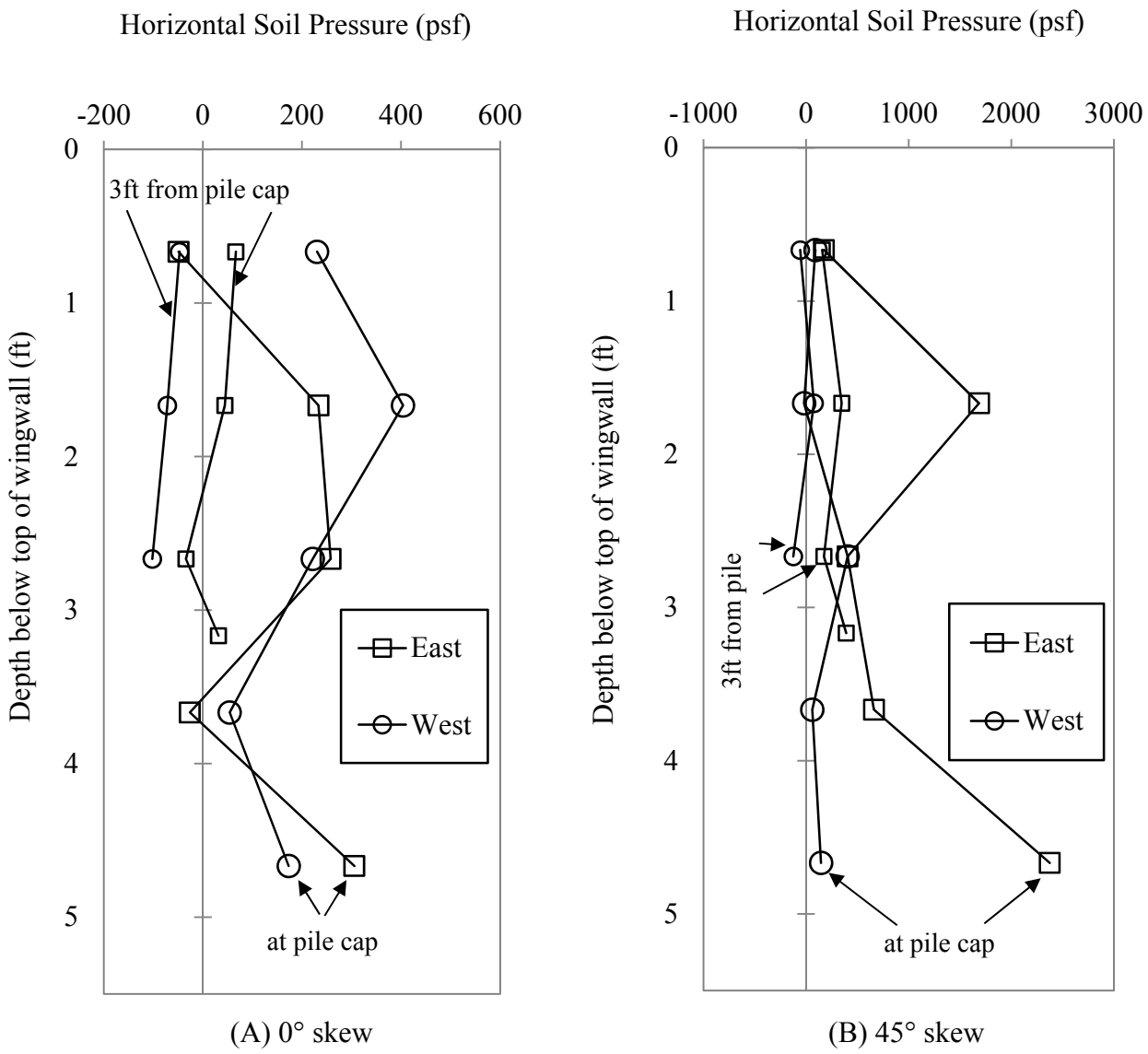

Figure 33. Soil pressure distributions on wingwalls at test completion: (A) 0° skew. (B) 45° skew.

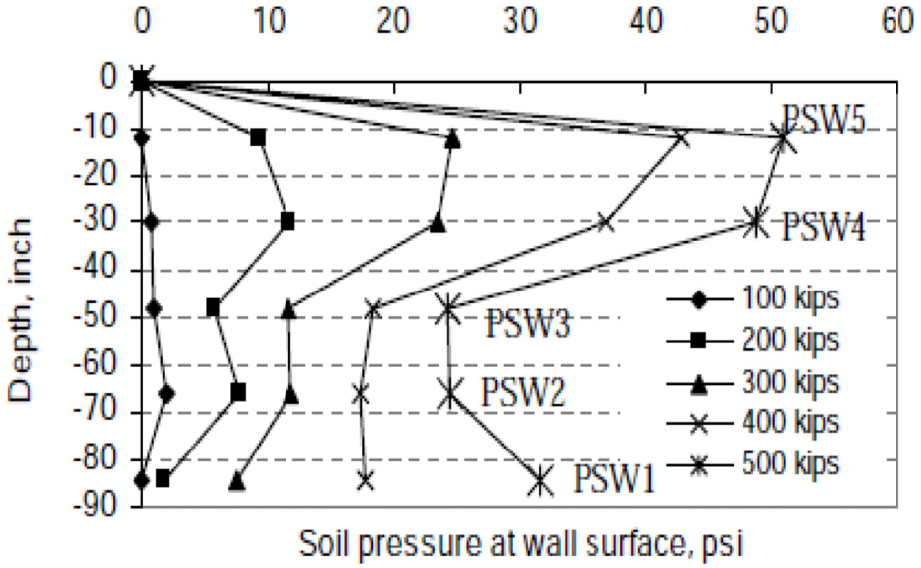

Distribution of soil pressure at west side of the wall surface vs. depth, Test 3

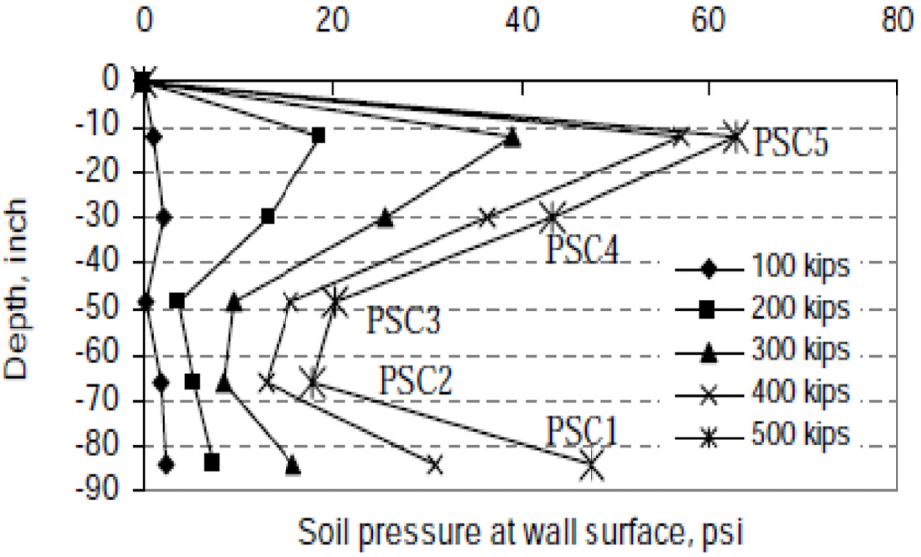

Distribution of soil pressure at center of the wall surface vs. depth, Test 3

Figure 34. Soil pressure at west end and center of abutment wall versus depth (Bozorgzadeh et al. 2008).

Lateral earth pressure coefficients (k) at the soil-wingwall interface were calculated using Equation **(14)** which divides the effective horizontal soil pressure by the initial vertical effective stress.

$$k = \frac{\sigma'_h}{\sigma'_{vo}} \tag{14}$$

Plots of the lateral earth pressure coefficients with depth are shown in Figure 35 for the non-skewed and 45° skewed abutments. The majority of k values at the soil-wingwall interface for the non-skewed abutment are less than 1, closer to at-rest conditions. On the 45° skewed abutment, however, the east wingwall is clearly experiencing higher lateral earth pressures with k values as high as 8.6 near the pile cap at a 20-in depth. The lateral pressures on the west wingwall are similar to the non-skewed case.

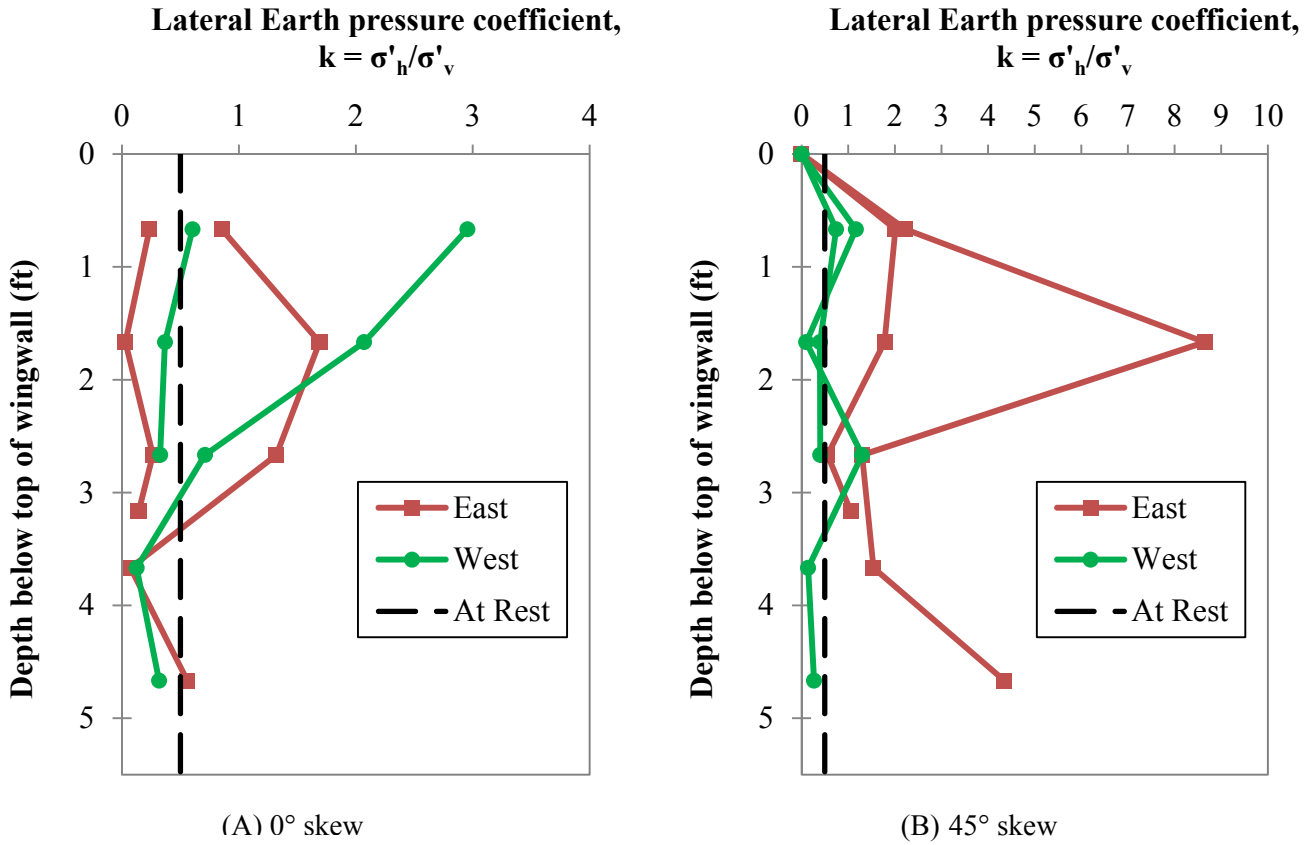

Figure 35. Lateral Earth pressure coefficient with depth along wingwalls for (A) 0° skew test and (B) 45° skew test (E = East; W = West).

CONCLUSIONS

Based on results from large-scale lateral load tests on abutments with longitudinal reinforced concrete wingwalls and subsequent computer analyses, the following conclusions can be draw:.

1. Large-scale field test results tests largely confirm previous results obtained from numerical models prepared by Shamsabadi et al. (2006) and small-scale lab tests by Jessee (2012) showing a significant reduction in peak passive force as skew angle increases (50% reduction for a 45° skew).
2. A reduction in peak passive force for abutments with longitudinal reinforced concrete (RC) wingwalls can be reasonably estimated with the reduction curve proposed by Rollins and Jessee (2012). A 50% reduction was measured compared to the recommended 65% reduction for 45° skew.
3. Observations of the failure plane and heave patterns suggest that a log-spiral failure geometry developed in the backfill. However, the 3D effects from shearing beyond the edges of the cap were less pronounced than for the unconfined or transverse wingwalls. Presumably, the parallel RC wingwalls inhibited the formation of these 3D shear surfaces to some extent.
4. The maximum moment acting on RC wingwalls was measured at the strain gauge located 20 in (50.8 cm) below the top of the wingwall nearest to the backwall at the mid-height of the tapered wall. For the 45° skewed abutment the maximum wingwall moment was 14x larger on the obtuse side of the abutment compared to the acute side and 7x larger compared to the maximum moment from the non-skewed abutment.
5. Lateral soil pressures were significantly higher on the east (obtuse side) wingwall compared to the west (acute side) wingwall on the 45° skewed abutment. Soil pressure distributions acting on non-skewed wingwalls were similar in magnitude to the west (acute side) wingwall on the 45° skewed abutment.

ACKNOWLEDGMENTS

Funding for this study was provided by an FHWA pooled fund study supported by Departments of Transportation from the states of California, Minnesota, Montana, New York, Oregon, and Utah. Utah served as the lead agency with David Stevens as the project manager. This support is gratefully acknowledged; however, the opinions, conclusions and recommendations in this paper do not necessarily represent those of the sponsoring organizations. We also express appreciation to the Salt Lake City Airport Department for providing access to the test site used in this study.

REFERENCES

AASHTO (2011). *Guide Specifications for LRFD Seismic Bridge Design*.

AASHTO (2011). "Guide Specifications for LRFD Seismic Bridge Design." 3-106.

Apirakyorapinit, P., Mohammadi, J., and Shen, J. (2012). "Analytical Investigation of Potential Seismic Damage to a Skewed Bridge." *Practice Periodical on Structural Design and Construction*, 16(1), 5-12.

Bozorgzadeh, A., Ashford, S. A., Restrepo, J. I., and Nimityongskul, N. (2008). "Experimental and Analytical Investigation on Stiffness and Ultimate Capacity of Bridge Abutments." University of California, San Diego.

Burke Jr., M. P. (1994). "Semi-Integral Bridges: Movements and Forces." 1-7.

Caltrans, C. D. o. T. (2010). "Seismic Design Criteria, Version 1.6, November 2010." Division of Engineering Services, Office of Structure Design, Sacramento, California.

Cole, R., and Rollins, K. (2006). "Passive Earth Pressure Mobilization during Cyclic Loading." *Journal of Geotechnical and Geoenvironmental Engineering*, 132(9), 1154-1164.

Duncan, J., and Mokwa, R. (2001). "Passive Earth Pressures: Theories and Tests." *Journal of Geotechnical and Geoenvironmental Engineering*, 127(3), 248-257.

Elnashai, A. S., Gencturk, B., Kwon, O., Al-Qadi, I. L., Hashash, Y., Roesler, J. R., Kim, S. J., Jeong, S., Dukes, J., and Valdivia, A. (2010). "The Maule (Chile) Earthquake of February 27, 2010: Consequence Assessment and Case Studies." Department of Civil and Environmental Engineering, University of Illinois at Urbana-Champaign, 190.

Lee, K. L., and Singh, A. (1971). "Relative Density and Relative Compaction." *Journal of Soil Mechanics and Foundations Design*, 97(7), 1049-1052.

Lemnitzer, A., Ahlberg, E., Nigbor, R., Shamsabadi, A., Wallace, J., and Stewart, J. (2009). "Lateral Performance of Full-Scale Bridge Abutment Wall with Granular Backfill." *Journal of Geotechnical and Geoenvironmental Engineering*, 135(4), 506-514.

Rollins, K., and Sparks, A. (2002). "Lateral Resistance of Full-Scale Pile Cap with Gravel Backfill." *Journal of Geotechnical and Geoenvironmental Engineering*, 128(9), 711-723.

Rollins, K. M., and Cole, R. T. (2006). "Cyclic Lateral Load Behavior of a Pile Cap and Backfill." *Journal of Geotechnical and Geoenvironmental Engineering, ASCE*, 132(9), 1143-1153.

Rollins, K. M., Gerber, T., Cummins, C., and Herbst, M. (2009). "Monitoring Displacement vs. Depth in Lateral Pile Load Tests with Shape Accelerometer Arrays." *Proceedings of 17th International on Soil Mechanics & Geotechnical Engineering*, 3, 2016-2019.

Rollins, K. M., Gerber, T. M., and Heiner, L. (2010). "Passive Force-Deflection Behavior for Abutments With MSE Confined Approach Fills." Brigham Young University Department of Civil & Environmental Engineering, Salt Lake City, UT, 83.

Rollins, K. M., and Jessee, S. (2012). "Passive Force-Deflection Curves for Skewed Abutments." *Journal of Bridge Engineering*, 17(5).

Romstad, K., Kutter, B., Maroney, B., Vanderbilt, E., Griggs, M., and Chai, Y. H. (1996). "Longitudinal Strength and Stiffness Behavior of Bridge Abutments." University of California, Davis, California.

Sandford, T. C., and Elgaaly, M. (1993). "Skew Effects on Backfill Pressures at Frame Bridge Abutments." *Transportation Research Record: Journal of the Transportation Research Board*, 1-11.

Shamsabadi, A., Kapuskar, M., and Zand, A. (2006). "Three-Dimensional Nonlinear Finite-Element Soil-Abutment Structure Interaction Model for Skewed Bridges." *5th National Seismic Conference On Bridges and Highways*, FHWA, ed.San Francisco, CA, 1-10.

Steinberg, E., and Sargand, S. (2010). "Forces in Wingwalls from Thermal Expansion of Skewed Semi-Integral Bridges." *Report No. FHWA/OH-2010/16*, Prepared by Ohio University for Ohio Department of Transportation, Athens, OH, 87.

Strassburg, A. N. (2010). "Influence of Relative Compaction on Passive Resistance of Abutments with Mechanically Stabilized Earth (MSE) Wingwalls." Master of Science, Brigham Young University, Provo, Utah.

Unjohn, S. "Repair and Retrofit of Bridges Damaged by the 2010 Chile, Maule Earthquake." *Proc., International Symposium on Engineering Lessons Learned from the 2011 Great East Japan Earthquake*.